*Research Paper*

# *In vivo* low-intensity magnetic pulses durably alter neocortical neuron excitability and spontaneous activity

*Short title: LI-rTMS alters cortical excitability in vivo*

Manon Boyer[1,2], Paul Baudin[2], Chloé Stengel[3], Antoni Valero-Cabre[3], Ann M. Lohof[1], Stéphane Charpier[2], Rachel M. Sherrard[1†*], Séverine Mahon[2†]

[1]Sorbonne Université & CNRS, IBPS-B2A, UMR 8256 Biological Adaptation and Ageing, Paris 75005, France

[2]Sorbonne Université, Paris Brain Institute–ICM, INSERM, CNRS, APHP, Pitié-Salpêtrière Hospital, team 'Network Dynamics and cellular excitability', Paris 75013 France

[3]Sorbonne Université, Paris Brain Institute–ICM, INSERM, CNRS, Pitié-Salpêtrière Hospital, team Cerebral Dynamics, Plasticity and Rehabilitation Group, FRONTLAB team, Paris 75013, France.

*Corresponding author:
Rachel M Sherrard
UMR 8256 B2A Biological Adaptation and Ageing
Boite 256, Sorbonne Université
9 Quai St Bernard, 75005, Paris

email: rachel.sherrard@sorbonne-universite.fr

† These authors contributed equally to this work

**Abstract**

Magnetic brain stimulation is a promising treatment for neurological and psychiatric disorders. However, a better understanding of its effects at the individual neuron level is essential to improve its clinical application. We combined focal low-intensity repetitive transcranial magnetic stimulation (LI-rTMS) to the rat somatosensory cortex with intracellular recordings of subjacent pyramidal neurons *in vivo*. Continuous 10 Hz LI-rTMS reliably evoked neuronal firing at ~4-5 Hz during the stimulation period, and induced durable attenuation of synaptic activity and spontaneous firing in cortical neurons, through membrane hyperpolarization and a reduced intrinsic excitability. However, inducing firing in individual neurons by repeated intracellular current injection did not reproduce LI-rTMS effects on neuronal properties. These data provide novel understanding of mechanisms underlying magnetic brain stimulation showing that, in addition to inducing biochemical plasticity, even weak magnetic fields can activate neurons and enduringly modulate their excitability.

## MAIN TEXT

### Introduction

Repetitive transcranial magnetic stimulation (rTMS) is a promising tool for the treatment of neurological and psychiatric diseases (*1*, *2*). However, a better understanding of the cellular mechanisms underlying rTMS effects is needed to optimize current treatment protocols, whose outcomes remain variable (*1*). Clinical application of magnetic stimulation involves the delivery of repeated high-intensity (0.5–2 Tesla, T) magnetic pulses to a targeted cortical area, which induce an electric field in the underlying brain tissue to activate cortical neurons and initiate activity-dependent plasticity (*3*, *4*). Such plasticity is confirmed in rodent organotypic cultures and brain slices, which showed that high-intensity magnetic stimulation induces synaptic plasticity in hippocampal networks (*5*, *6*) and modulates neocortical inhibitory interneurons (*7*, *8*).

Beside the use of high-field magnetic stimulation, whose duration and frequency of application is limited by technical and safety reasons (*2*), a new generation of protocols using low-intensity (milliTesla, mT) magnetic fields is emerging. Human studies show that low-intensity stimulation to the entire brain can modulate EEG activity and cerebral function (*9–11*). Moreover, focal application of these weak stimuli (low-intensity rTMS; LI-rTMS) in rodents facilitates the reorganisation of abnormal circuits (*12*, *13*), stimulates axonal growth and synaptogenesis (*14*), and modifies cellular calcium signalling and gene expression (*14*, *15*). However, low-intensity stimulation generates electric fields below those considered to initiate action potential firing (*16–18*), thus it remains unclear how LI-rTMS induces plasticity at the single cell level, to contribute to functional and structural changes. Moreover, the impact of LI-rTMS on the electrical properties of cortical neurons *in vivo*, *i.e.* in an experimental condition that preserves neuronal connectivity and allows physiologically relevant spontaneous activity, is still unknown. Such information is

78 necessary to understand the cellular basis of human rTMS effects, wherein cortical
79 responses to magnetic stimulation critically depend on the ongoing activity of the stimulated
80 brain region (*3*, *19*).

81 To fill this gap, we developed a new *in vivo* model for delivering low-intensity (10
82 mT) focal rTMS in the sedated rodent during intracellular recording of identified neurons.
83 In these conditions, we can explore the online and after-effects of LI-rTMS on the electrical
84 membrane properties of single cortical neurons within an intact stimulated network. Our
85 findings provide direct evidence that low-intensity magnetic pulses applied to the
86 somatosensory cortex (S1) reliably elicit action potentials (APs) in pyramidal cells. We also
87 demonstrate that a 10-minute period of continuous 10 Hz LI-rTMS produces long lasting (≥
88 40 minutes post-stimulation) modifications in intrinsic membrane properties and
89 spontaneous activity. These after-effects include dampening of resting membrane
90 properties, substantial membrane hyperpolarization, and weakening of background synaptic
91 and firing activity. This was accompanied by altered transfer function, characterized by an
92 increase in the minimal current required to induce neuronal firing. These LI-rTMS-mediated
93 effects were not reproduced by a 10-minute period of firing elicited by intracellular injection
94 of current pulses at 10 Hz. Our data show that, like high-intensity stimulation, LI-rTMS
95 activates neurons and durably modulates their activity and excitability. This changes the
96 paradigm for brain stimulation with weak magnetic fields, and increases the range of
97 potentially therapeutic stimulation parameters for clinical use.

98

99 **Results**

00
01 To study the immediate and time-dependent effects of LI-rTMS on cortical activity, we
02 coupled *in vivo* intracellular recordings of S1 neurons ($n$ = 41 from 31 rats) with the
03 monitoring of the corresponding ECoG (Fig. 1, A–C). Some recorded neurons were loaded

with neurobiotin ($n$ = 19) and confirmed histologically to be pyramidal neurons located in either layer 5 ($n$ = 11) or 2/3 ($n$ = 8; Fig. 1B). All recorded neurons displayed the distinctive firing profiles of S1 pyramidal cells (*20*, *21)*: either regular spiking ($n$ = 27; Fig. 3B) or intrinsic bursts of APs ($n$ = 14) in response to injection of suprathreshold current pulses (Fig. 3B and fig. S1). Since no differences in LI-rTMS effects were observed between pyramidal neurons located in layers 2/3 or layer 5, we pooled the corresponding results.

**LI-rTMS decreases spontaneous activity of cortical neurons**

In a first group of S1 cortical neurons, we verified the stability of our recordings by measuring variations in several electrical membrane properties over a 20-minute period preceding the application of LI-rTMS (Fig. 1C and fig. S1). During this control period, the TMS coil was already positioned above S1 but no stimulation was delivered. As illustrated in figure S1, we did not find any significant changes in neuronal spontaneous activity or membrane excitability during this baseline period (see Supplementary information for details). To analyze the time-dependent effects of LI-rTMS ($n$ = 16 experiments), we divided our recordings into five consecutive periods: 1) a pre-stimulation time (Pre), being the 10 minutes immediately before LI-rTMS; 2) 10 minutes of LI-rTMS at 10 Hz; and 3) three successive post-stimulation times: 10–20 min (P1), 20–30 min (P2) and 40–50 min (P3) after the start of the LI-rTMS (Fig. 1C).

Spontaneous intracellular activity during the pre-stimulation period was characterized by broadband frequency synaptic fluctuations of small amplitude, leading to a Gaussian-like distribution of membrane potential (Vm) values around a mean (± SD) of -72.1 ± 4.8 mV ($n$ = 16 neurons) (Fig. 1C, Pre and Fig. 2, A and B). This background synaptic activity caused spontaneous firing in half of the recorded neurons ($n$ = 8 out of 16), with a mean frequency of 1.8 ± 2.3 Hz ($n$ = 8) and high temporal variability (CV2 ISIs = 1.2 ± 0.3,

29 $n$ = 8) (Fig. 1C and 2A). Consistent with this intracellular pattern of activity, the ECoG
30 profile appeared desynchronized and composed of relatively fast, small-amplitude cortical
31 waves (Fig. 1C), as classically observed under sufentanil sedation (*22*, *23*).

32 Our first observation was that 10 minutes LI-rTMS at 10 Hz provoked a progressive
33 polarization of Vm in all tested neurons (Fig. 2, A to C). Compared to Pre, a net membrane
34 hyperpolarization was already present immediately after LI-rTMS (P1: -2.3 ± 2.0 mV, $n$ =
35 16 neurons; $P < 0.01$) and persisted until the end of the recording (P3: -2.3 ± 1.9 mV, $n$ = 9
36 neurons; $P < 0.01$) (Fig. 1Cb and Fig. 2, A to C), resulting in a negative shift of the Vm
37 distribution during the post-stimulation periods (Fig. 2 B left). The amplitude of background
38 synaptic activity, quantified as the standard deviation of Vm values, was also reduced after
39 LI-rTMS in both active and silent neurons (Fig. 2A), reaching a 10.8 ± 12.2 % decrease at
40 P3 as compared to the pre-stimulation period ($P < 0.01$, $n$ = 9 neurons) (Fig. 2, A to C). This
41 was associated with a global decrease in the power of synaptic activity for frequencies below
42 10 Hz (Fig. 2, A and B). This dampening of synaptic noise amplitude was relatively
43 unexpected because the sustained Vm hyperpolarization would usually predict increased
44 driving force of synaptic currents and therefore larger synaptic potentials, particularly
45 because there was no inward membrane rectification in the voltage-current ($V$-$I$)
46 relationships in our recorded cells (fig. S1Bb).

47 Consistent with the attenuation of intracellular synaptic events and cell polarization,
48 the spontaneous firing of these cortical neurons was markedly reduced after LI-rTMS. Five
49 of the 8 active neurons prior to LI-rTMS became completely silent by P2, while the firing
50 of the 3 remaining cells reached a mean frequency of about 0.07 ± 0.13 Hz at P3 (Fig. 2, A
51 and C). This failure of ongoing cell firing was not due to altered AP properties, as their
52 amplitude, half-width duration and voltage threshold did not differ between pre- and post-
53 stimulation periods (Fig. 2B, right and table S1). The post-LI-rTMS inhibition of

54 spontaneous activity was thus not due to changes in the ionic mechanisms underlying AP
55 generation. Instead, the decreased background synaptic drive is more likely to explain, at
56 least in part, the significant membrane hyperpolarization and the attenuated ongoing AP
57 firing.
58
59 **LI-rTMS alters neuronal integrative properties and input-output relationship**
60 We next tested if LI-rTMS altered the excitability of S1 pyramidal neurons by comparing
61 their integrative properties, *i.e.* their ability to process subthreshold membrane currents, and
62 their input-output relationship before and after stimulation.
63 We first examined changes in membrane input resistance (Rm) and membrane time
64 constant (τm), two parameters that govern, respectively, the ability of synaptic currents to
65 change Vm, and the efficacy with which a neuron summates synaptic potentials over time.
66 Rm values, extrapolated from the slope of the *V-I* curves (fig. S1B), were already
67 significantly reduced at P1 (compared to Pre: -14.1 ± 6.6 %, $n$ =11 neurons; $P < 0.001$), a
68 decrease that persisted for up to 40 min after the end of stimulation ($n$ = 9 neurons; $P <$
69 $0.01$) (Fig. 3, A and C). The decrease in Rm values was not caused by LI-rTMS-mediated
70 changes in the morphology of the recorded neurons, whose principal anatomical properties
71 were comparable to those classically reported for S1 pyramidal cells (*21*, *24*, *25*) (Fig. 1B).
72 τm values also showed a persistent decrease that closely matched the reduction in Rm (Fig.
73 3C). The attenuation of Rm and τm by LI-rTMS may contribute to the smaller amplitude of
74 spontaneous synaptic potentials and their ineffective summation to elicit APs.
75 As changes in Vm and Rm can affect the reactivity of a neuron to its inputs (*22*, *26*),
76 we then looked for possible LI-rTMS-induced modifications in the input-output
77 relationship. We injected positive current pulses of increasing intensity during the different
78 recording periods and counted the number of evoked APs, generating frequency-current (*F*-

79 *I*) curves (fig S1Cb and Fig. 3B). After LI-rTMS, *F-I* curves progressively shifted to the
80 right, leading to a ~50% increase of the baseline (Pre) threshold current values by P3 ($n = 7$
81 neurons; $P < 0.05$) (Fig. 3, B and C). This reduced neuronal responsiveness to small
82 excitatory inputs was accompanied by a relative stability of the neuronal gain, defined as
83 the slope of the linear portion of F-I curves, throughout the post-stimulation period ($P =$
84 $0.23$) (Fig. 3C).
85
86 **Low-intensity magnetic pulses trigger APs**
87 Decreased neuronal responsiveness to 10 Hz LI-rTMS is somewhat unexpected because *in*
88 *vitro* studies from rodents have shown that high- (1 Tesla) and medium- (85 mT) intensity
89 10 Hz rTMS increases the strength of excitatory synaptic transmission in hippocampal
90 networks (*5*) and potentiates the excitability of neocortical pyramidal neurons (*27*). Those
91 previous reports confirm results of studies in humans, where high-intensity rTMS (≥ 5 Hz)
92 increases cortical excitability, as measured by the amplitude of the evoked motor response
93 to a single TMS pulse delivered to the primary motor cortex (*1*, *2*).
94 To understand the mechanisms underlying the long-lasting inhibitory effects of LI-
95 rTMS on cortical activity and integrative properties, we investigated the immediate effects
96 of LI-rTMS during the stimulation period. A practical difficulty for this analysis arises from
97 the brief (~1.6 ms) large-amplitude artifacts generated by each LI-rTMS pulse (Figs. 1 and
98 4, and fig. S2), which obscures the early part of the neuronal response. However, we noticed
99 in all recorded neurons ($n = 16$) that the terminal part of many artifacts was rapidly followed
100 by a biphasic voltage waveform resembling an intracellular AP (Fig. 4A and fig. S2A). We
101 thus removed the stimulation artifacts off-line from traces displaying an apparent AP
102 waveform by cutting a 1.6 ms period at the onset of each magnetic pulse and interpolating
103 the missing data with a straight line (Figs. 4 and 5, and fig. S2 for details). The artifact-free

recordings revealed intracellular waveforms whose shape, peak amplitude and kinetics matched those of spontaneous APs recorded from the same neurons (Fig. 4 Ab). The mean latency of AP-like events, calculated from the end of the stimulus to the peak of the waveform, was 0.6 ± 0.1 ms ($n$ = 16 neurons) and the percentage of individual magnetic pulses immediately preceding these waveforms was 24 ± 31 % ($n$ = 16 neurons; Fig 4B, bottom left), with a high cell-to-cell variability (from 0.3 to 99.8 %). Given that magnetic intensity decreases by distance-squared, we tested whether this inter-neuronal variability, i.e. the success rate of magnetic pulse-induced APs depended on the depth of recorded cells; there was no correlation ($r^2$ = 0.03). Notably, these AP-like events are not non-biological artifacts resulting from direct action of the magnetic field on the recording electrode: they did not occur in control experiments in which a model cell was used to simulate the recording of a pyramidal neuron (fig. S2B).

To confirm that the high-voltage waveforms were indeed APs, we tested their sensitivity to sustained Vm hyperpolarization, which prevents firing by bringing the neuron's membrane potential further from the AP threshold, or to the blockade of voltage-gated sodium channels by the lidocaine analog QX-314.

First, short periods of *DC* hyperpolarization (from -0.1 to -2 nA) were applied during the control period or during LI-rTMS, and their effects on the rate of spontaneous APs and LI-rTMS-induced AP-like events were measured (Fig. 4B). In the absence of magnetic stimulation, spontaneous firing frequency in this subset of neurons was 1.8 ± 1.6 Hz at rest (Vm = -71.9 ± 7.0 mV, $n$ = 6 neurons). This rate progressively declined with imposed membrane hyperpolarization, and fell to zero when Vm reached -81.2 ± 8.1 mV ($n$ = 6 neurons) (Fig. 4B, top). This Vm hyperpolarization was associated with an increased amplitude of synaptic fluctuations, as expected from the greater driving force of excitatory synaptic currents (Fig. 4B, top right). Hyperpolarizing the same cortical neurons during

229 short periods of LI-rTMS similarly decreased the rate of the AP-like events, from 4.0 ± 2.7
230 Hz at rest ($n$ = 6 neurons) to a very low residual rate of 0.04 ± 0.05 Hz at the most negative
231 level of membrane polarization tested (Vm = -81.2 ± 8.1 mV, $n$ = 6 neurons) (Fig. 4B,
232 bottom). In both control and LI-rTMS conditions, spontaneous AP firing was restored at the
233 end of the *DC* current injection (not shown).

234 Second, to test whether the putative LI-rTMS-induced APs had the same ionic
235 mechanisms as spontaneous APs, we perfused the intracellularly recorded neurons with QX-
236 314 ($n$ = 9) and compared the drug-related changes in amplitude of both types of APs. In
237 each neuron, measurements were made during alternating control and stimulation periods
238 of 5–160 seconds. The peak potential of spontaneous APs was progressively reduced ($P <$
239 $0.05$) by the QX314 (Fig. 4C) and this time-dependent reduction in peak amplitude was
240 accompanied by a mean Vm depolarization of 5–10 mV, as classically observed in QX-314-
241 filled cortical neurons (*28*, *29*). The decrease in peak values of LI-rTMS-induced waveforms
242 and spontaneous APs was almost identical at any time after the onset of QX-314 diffusion
243 ($P > 0.2$ for each recording time), reaching ~ -14–20 mV in the neurons that could be
244 recorded until 30–40 min after cell impalement ($n$ = 5) (Fig. 4C). Because the QX314-
245 reduced APs were occasionally difficult to distinguish from spontaneous depolarized
246 synaptic potentials in recordings of long duration (Fig. 4Ca, arrows), we also examined the
247 effects of QX-314 on APs evoked by depolarizing current steps (0.2–0.4 nA, $n$ = 9 neurons)
248 (Fig. 4, Cb and Cc). Again, the time-course of the reduction in current-induced AP peak
249 potentials was similar to that measured for LI-rTMS-induced APs ($P > 0.1$ for each
250 recording time) (Fig. 4, Cb and Cc).

251 The LI-rTMS-induced APs occurred in all recorded cortical neurons, regardless of
252 their firing frequency prior to stimulation (Fig. 5, A to C). This led to a significant increase
253 in the overall firing rate (including both spontaneous and LI-rTMS-evoked APs) throughout

the stimulation period ($n$ = 16 neurons; $P < 0.05$) (Fig. 5B). However, we found that the rate of spontaneous APs, when measured separately, was decreased by almost 45% during LI-rTMS (Pre: 1.8 ± 2.3 Hz, $n$ = 8 active neurons, LI-rTMS: 0.6 ± 0.8 Hz, $n$ = 8 neurons; $P <$ 0.01) (Fig. 5B). The induced APs did not result from a LI-rTMS-mediated increase in synaptic activity or sustained membrane depolarization since the examination of artifact-free records did not show significant change in the amplitude of Vm fluctuations in association with the firing induced by magnetic pulses (Figs. 4 and 5, and fig. S2A). However, their short latency and ability to be evoked from relatively hyperpolarized membrane potentials indicate that LI-rTMS-evoked APs probably resulted from activation of an axonal site located close to the soma.

These results demonstrate for the first time that 10 Hz LI-rTMS can elicit AP firing in pyramidal neurons, with kinetic and ionic mechanisms similar to spontaneous APs, despite inducing an electric field estimated to be at least 100 times lower than that used in high-intensity rTMS. Moreover, these data demonstrate at the individual neuron level that a 10-minute session of continuous 10 Hz LI-rTMS produces robust and long-lasting inhibitory effects on the activity and integrative properties of pyramidal neurons.

**Action potentials evoked by intracellular current injection do not reproduce LI-rTMS effects**

In order to determine whether the firing induced by magnetic stimuli was solely responsible for the changes in cortical neuron activity and responsiveness, we examined, in another group of S1 neurons, the impact of an AP discharge evoked by intracellular injection of current steps. Cortical neurons ($n$ = 7) were thus challenged with repetitive depolarizing current pulse stimulation (rCPS) applied at 10 Hz for 10 min (Fig. 6A). The intensity of the

intracellularly injected current was adjusted in each neuron to obtain a proportion of suprathreshold stimulations (~30%) and an overall firing frequency comparable to those produced by LI-rTMS (5.9 ± 4.6 Hz, $n = 7$ neurons, including both spontaneous and evoked APs; $P > 0.4$) (Fig. 6B). The effects of rCPS were compared to a subgroup of magnetically stimulated neurons ($n = 9$) with similar baseline membrane electrical properties, including mean Vm, spontaneous firing frequency and Rm ($n = 9$; $P > 0.1$ for each parameter).

The first obvious difference distinguishing the effects of rCPS and LI-rTMS was that current-evoked APs did not produce neuronal hyperpolarization after the stimulation period (Fig. 6C, left and fig. S3D). This absence of change in mean Vm was accompanied by stable Vm fluctuation and spontaneous firing frequency (Pre *versus* post-rCPS: $P > 0.2$ for each parameter) (Fig. S3, A and D). Furthermore, comparison of *V-I* curves before and after rCPS did not indicate significant modification of Rm (Pre, 17.2 ± 6.9 MΩ, $n = 6$ neurons *vs.* Post, 17.9 ± 7.5 MΩ, $n = 6$ neurons; $P = 0.14$) or τm (Pre, 6.5 ± 1.8 ms, $n = 6$ neurons vs. Post, 6.3 ± 1.6 ms, $n = 6$ neurons; $P = 0.28$) (Fig. 6C, middle and fig. S3, B and D). Finally, analysis of *F-I* curves obtained after application of the 10 Hz current pulses revealed heterogeneous modification in the sensitivity of cortical neurons to weak depolarizing inputs. Although average current threshold values did not significantly change ($P = 0.4$), the majority of neurons ($n = 4$ out of 6 tested cells) exhibited a significant decrease in their firing threshold (ΔIth = -0.14 ± 0.07 nA, $n = 4$; $P < 0.05$) during the post-stimulation period. This variable rCPS-induced modulation of cortical neuron responsiveness was not accompanied by modification in the neuronal gain ($P > 0.4$) (Fig. 6C, right and fig. S3, C and D).

These data indicate that the firing of single cortical neurons at a similar frequency to that induced by magnetic stimulation (~ 5 Hz) is not sufficient to reproduce, on its own, the LI-rTMS-related changes in neuronal excitability.

## Discussion

To our knowledge, our study is the first to investigate the immediate (online) and after- (offline) effects of low-intensity rTMS on the electrical properties of single neurons *in vivo*. Because rTMS-induced cortical responses depend on the ongoing brain state (*3*, *19*, *30*), we explored the impact of LI-rTMS in rats sedated with sufentanil to retain stable background cortical activity, similar to the waking state, during the long intracellular recordings (*22*, *31*, *32*). Our results indicate that a single 10-minute period of continuous 10 Hz LI-rTMS alters the passive membrane properties of S1 pyramidal neurons, reduces their intrinsic excitability and attenuates their spontaneous firing. These cellular changes were present immediately after the end of stimulation and persisted for at least 40 min. We also found that low-intensity magnetic pulses were able to trigger APs in all recorded neurons. These findings deepen our knowledge on the cellular mechanisms underlying LI-rTMS-induced plasticity and may guide the development of new stimulation patterns for clinical treatment.

### LI-rTMS induces action potentials in stimulated neurons

A major and unexpected finding of the present study was the discovery that, during stimulation, low intensity (10 mT) magnetic pulses were able to elicit APs in all recorded pyramidal cells (25% of pulses on average). This challenges the common assumption that the strength of the electrical field induced in brain tissue by LI-rTMS is much weaker than that required for neuronal activation, and that low-intensity magnetic pulses only act through subthreshold mechanisms, such as shifting the level of cell polarization (*16–18*). Our result is however coherent with extracellular recordings from retinal ganglion cells *in vitro* showing short latency spiking in response to weak electric fields (*33*) and a recent study observing in rat brain slices that a single medium-intensity (60 mT) magnetic stimulus

causes a rapid and transient activation of voltage-sensitive sodium currents and facilitates AP firing in S1 pyramidal neurons (*34*).

The mechanisms by which individual magnetic pulses activate neurons remain unclear. Neuronal firing induced by high-intensity TMS is thought to result either from trans-synaptic or direct depolarization of specific neuronal compartments and to be initiated from an axonal site located more or less close to the soma (Ref *35*, *36* and references therein). We showed that LI-rTMS-induced APs had a short latency relative to the magnetic stimulus, were not associated with an increase in the amplitude or frequency of subthreshold excitatory synaptic events and could be triggered even from a hyperpolarized Vm. This supports AP initiation through direct activation of the axon initial segment, which has a lower AP threshold due to its high concentration in voltage-gated sodium channels (*37*, *38*).

We found that the percentage of magnetic pulses initiating APs varied between cells, which could reflect differences in the baseline electrophysiological or morphological properties among the recorded pyramidal neurons. Indeed, calcium imaging of primary hippocampal cultures (*39*) and patch-clamp recordings from motor cortex slices (*17*) revealed diverse pyramidal neuron sensitivity to magnetic and electric fields, depending on their location, morphology and intrinsic excitability. Furthermore, natural fluctuations in baseline pyramidal neuron spontaneous firing could also influence their responsiveness to magnetic stimuli, as previously observed with extracellular recordings in the cat visual cortex following high-intensity rTMS (*40*). Finally, because the electric field induced by TMS decays with distance in the extracellular space (*41*), the relative space between the stimulating coil and each recorded neuron may also contribute to response variability.

**Continuous 10 Hz LI-rTMS durably decreases cortical excitability and activity**

The main after-effects observed in neocortical pyramidal neurons following continuous 10 Hz LI-rTMS included a decrease in the amplitude of background synaptic noise, substantial membrane hyperpolarization and marked reduction or cessation of spontaneous firing. These changes in spontaneous activity were accompanied by an attenuation of the integrative properties of cortical cells (correlated decrease in Rm and τm) and an alteration of their intrinsic excitability (increase in the minimal current firing threshold).

Our data reveal some characteristics of LI-rTMS effects that allow us to differentiate between an origin that is primarily associated with changes to synaptic events or intrinsic cellular properties. Long-term depression of synaptic inputs onto the recorded neurons, which could explain the observed reduction in synaptic activity, would decrease global membrane conductance (due to smaller excitatory synaptic conductance) and thus increase Rm and τm values (*42*) – the opposite of our findings. Rather, we suggest that LI-rTMS-mediated inhibition of neuronal activity originates from an alteration of the integrative properties of each cortical pyramidal neuron. Indeed, the initial reduction in Rm and τm, which attenuates neuronal responsiveness to their synaptic inputs, could explain both the reduced amplitude of Vm fluctuations and membrane hyperpolarization. Given the inverse correlation linking current firing threshold to Vm in cortical neurons (*22*, *43*), the increased cell membrane polarization could in turn explain the rightward shift of input-output relations and the reduced intrinsic excitability. Finally, all these cellular modifications will combine to reduce the efficiency with which cortical neurons process synaptic currents and generate APs and, thus, explain the progressive decrease of spontaneous firing. This weakening of firing in individual neurons will contribute to global reduction of the flow of synaptic activity within the stimulated cortical network, which will further reduce synaptic and firing

activity. In addition, an increased activity of neocortical GABAergic interneurons could also contribute to the reduction of pyramidal cell activity, by producing a robust shunting effect on pyramidal neurons membrane (*44*) and participating to the reduced Rm (due to larger inhibitory synaptic conductance).

The precise subcellular mechanisms through which LI-rTMS exerts its effects warrant further investigation. However, we hypothesize that there is a contribution from increased neuronal firing during stimulation that opens voltage-gated calcium channels, and increases intracellular calcium concentration to activate calcium-dependent enzymatic cascades and downstream regulation of ionic conductances (*45*, *46*). In line with this hypothesis, pyramidal neuron firing induced by medium-intensity (60 mT) rMS *in vitro* is associated with increased cytosolic calcium (*34*). Moreover, our data showing changes in Rm and current firing threshold together with stable neuronal gain after LI-rTMS, suggest that the long-lasting decrease in neuronal excitability is mediated by the modulation of potassium currents activated around resting membrane potential (*47*). This suggestion is supported by previous reports, in which similar depression of intrinsic cell excitability was attributed to calcium-dependent upregulation of slowly-inactivating potassium currents (*48*, *49*).

Although the LI-rTMS-induced pyramidal cell firing provides a potential explanation for their reduced excitability, our results also indicate that induced APs, and their associated changes in calcium concentration, may not be sufficient to trigger the time-dependent post-stimulation effects we see in cortical neurons. Simply replicating the level of LI-rTMS-induced AP firing by repeated intracellular injection of current pulses in single neurons did not produce any significant modifications in resting and active membrane properties. This absence of neuromodulation in the presence of electrically-induced APs is consistent with electric field-induction being only one of several mechanisms activated by

electromagnetic pulses. We have previously shown that cryptochrome magnetoreceptors are required for neuroplasticity effects of LI-rTMS (*14*) and modulate reactive oxygen species (ROS) (*50*). In cell redox physiology, ROS activate ryanodine receptors to release calcium from intracellular stores (*51*), a phenomenon we have demonstrated in cortical neurons in response to LI-rTMS (*15*). It is therefore likely that activation of both voltage-gated calcium channels and release of calcium from intracellular stores is required for the long-term modulation of pyramidal neuron activity.

**Relevance of LI-rTMS to human rTMS treatment**

The LI-rTMS-induced inhibitory effects on neuronal excitability and firing is surprising in light of former studies using high-intensity rTMS. According to these reports, high-frequency magnetic stimulation (≥ 5 Hz) is expected to increase cortical excitability (*1*, *52–54*), potentiate excitatory synaptic transmission or upregulate the expression of neurochemical markers of synaptic plasticity (*5*, *30*, *53*, *55*).

However, there are important differences between these works and the current investigation, which can explain the different outcomes. First, in some of these studies, rTMS effects on synaptic function were examined *ex vivo* after the application of repeated daily sessions of high-frequency rMS (*30*, *53*), which is not the case here. Second, in studies where acute effects of magnetic stimulation were measured, the rMS was usually delivered directly to a brain slice or organotypic slice cultures and not to an intact brain as in our *in vivo* experimental condition (*5*, *27*, *55*). For example, in mouse S1 slices, 3 minutes of medium-intensity (85 mT) intermittent theta-burst magnetic stimulation was shown to reduce AP voltage threshold in pyramidal neurons and increase their current-evoked firing, without changing resting membrane properties (*27*). Discordance between results obtained *in vitro* and in living brains has already been described in studies of activity-dependent

synaptic plasticity. We previously reported that opposite changes in synaptic efficacy can be induced, at the same synapses and in response to the same stimulation paradigm, *in vivo* and *in vitro* (*56*). Therefore, the differences between previous observations and our current *in vivo* findings further support the dependence of rTMS outcomes on the ongoing activity in the influenced neural networks at the time of the stimulation (*1*, *30*). Finally, most previous studies used magnetic fields at least ten times stronger than the one used in our study. High-frequency stimulation protocols at high-intensity require regular pauses to allow for cooling of the coil – resulting in short periods (a few seconds) of stimulation separated by pauses without stimulation (see Ref *53*, *54* for reviews), an intermittent pattern in contrast to our continuous 10 Hz. The contrasting effects of continuous and intermittent pulse delivery has been shown for theta-burst stimulation, which induces opposite effects on the amplitude of motor-evoked potentials in response to single TMS pulse in humans (*52*). Thus, consistent with the degree of structural and biochemical plasticity induced by LI-rTMS being highly dependent on stimulation parameters (*14*, *15*), the importance of stimulation pattern on the magnitude and polarity of excitability modulation cannot be overstated.

Although the functional consequences of LI-rTMS-mediated depression of cortical excitability for S1 network function and behavior remain unknown, we hypothesize that our continuous 10 Hz LI-rTMS protocol may be useful in the context of epileptic disorders, which are often associated with cortical hyperexcitability and paroxysmal network synchronization (*57*). An understanding of the immediate and lasting effects on neuronal activity, measured in real time, is an important advance for the development and evaluation of stimulation patterns in future clinical treatments.

In summary, the novelty of our findings, that even weak magnetic fields can activate neurons and modulate their intrinsic excitability, changes our understanding of low-

intensity magnetic brain stimulation by showing that the more accessible low-intensity approaches have some underlying processes in common with already established high-intensity clinical treatments, but without the constraints of special high-voltage equipment. This knowledge not only expands the range of stimulation protocols (pulse frequency and patterns), and therefore future potential clinical treatments, but also renders LI-rTMS treatments available beyond the hospital setting.

**Fig. 1. Experimental paradigm and definition of recording periods.**

(**A**) Schematic representation of the experimental set-up illustrating the positions of the LI-rTMS coil and the recording electrodes. ECoG activity from rat barrel cortex (S1) was monitored during intracellular recording of subjacent pyramidal neurons (Intra S1). LI-rTMS (10 Hz for 10 minutes) was delivered through a 8-mm wire coil placed ~2 mm away from the brain surface. **(B)** Reconstruction of a layer 2/3 pyramidal neuron filled with neurobiotin during recording. The dotted line indicates separation between cortical layers 1 and 2/3. **(Ca)** Simultaneous ECoG and intracellular recordings from a layer 2/3 pyramidal neuron, during the baseline period (Pre), the stimulation protocol (LI-rTMS), and at different times (+10−20 min, P1; +20−30 min, P2; +40−50 min, P3) after the onset of LI-rTMS (Post). **(Cb)** Expanded view (500 ms) of the recordings shown in **(Ca)**. The LI-rTMS artifacts are shown in red. Here and in the following figures, the values of Vm are indicated at the left of intracellular records.

**Fig. 2. LI-rTMS causes lasting inhibition of cortical neurons spontaneous activity.** (**A**) Representative recordings of spontaneous intracellular activity of active (cell 1) and silent (cell 2) S1 neurons before LI-rTMS (Pre) and during the first (P1) and third (P3) post-stimulation periods. The associated time-frequency maps, after removal and interpolation of APs, are temporally-aligned below the records. (**B**) Left: probability densities of Vm values computed from cell 2 during the different periods (60 sec of recording, bin size 1 mV). Middle: mean (solid lines) ± SD (shaded areas) frequency power spectra computed from intracellular subthreshold signals in the pre- and post-stimulation periods ($n$ = 16 neurons) showing a progressive decrease in the power of the 5-10 Hz frequency band after LI-rTMS (Wilcoxon signed rank test with Benjamini-Hochberg's post hoc correction, comparing P1 and P3 with Pre). Right: superimposed examples of average ± SD (shaded areas) of spontaneous APs and corresponding phase-plots (inset) during Pre (black trace, $n$ = 138) and Post (blue trace, $n$ = 28) LI-rTMS periods. **(C)** Time-dependent changes in cortical spontaneous activity after 10 minutes LI-rTMS. **(Ca)** Time course of the mean change (black line) ± SD (gray shaded area) in Vm (after subtraction of the mean Pre value), in the amplitude of Vm fluctuation (σVm; after subtraction of the mean Pre value), and in the spontaneous firing frequency of active neurons (Spont. Firing), calculated over successive 30-second periods before and after LI-rTMS application (red rectangle). **(Cb)** Comparison of Vm, σVm and spontaneous firing rate values (mean ± SD) during baseline (Pre) and at the three post-LI-rTMS periods (P1, P2, P3) [RMANOVA and Bonferroni post-hoc comparisons; Vm: $n$ = 16, 16, 8 and 9, $F_{0.39, 3.89} = 12.35$, $P = 0.034$; σVm: $n$ = 16, 16, 8 and 9, $F_{1.36, 13.55} = 11.69$, $P = 0.0025$; spontaneous firing: $n$ = 8, 8, 3 and 3, $F_{1.64, 6.03} = 9.74$, $P = 0.015$]. Here and in the following figures, the gray circles in the pooled-data graphs indicate values for individual neurons. In (Ca) and (Cb), analysis of ongoing firing was restricted to neurons which were spontaneously active during baseline. *$P < 0.05$, ** $P < 0.01$, *** $P < 0.001$, ns: non-significant; ◊ = too few data for post-hoc comparison.

**Fig. 3. LI-rTMS negatively alters resting integrative properties and intrinsic excitability.**

(**A**) Average ($n$ = 6–30 trials) voltage responses (upper traces) of an S1 pyramidal neuron to hyperpolarizing current steps of increasing intensity (-0.2 to -0.6 nA, lower traces) before (Pre) and after LI-rTMS (periods P1 and P3). (**B**) Current-evoked firing responses to depolarizing current pulses of increasing intensity recorded from anS1 neuron in Pre, P1 and P3 periods. (**C**) Population data showing the temporal evolution of mean (± SD) values of Rm, τm, current threshold ($I_{th}$) and neuronal gain (γ) values. [RMANOVA and Bonferroni post-hoc comparisons; Rm: $n$ = 11, 11, 8 and 9, $F_{0.14, 1.19} = 10.54$, $P = 0.08$; τm: $n$ = 11, 11, 8 and 9, $F_{1.61, 13.44} = 8.24$, $P = 0.006$; $I_{th}$: $n$ = 12, 11, 8 and 7, $F_{0.72, 5.55} = 16.91$, $P = 0.01$; γ: $n$ = 12, 11, 8 and 7, $F_{0.14, 1.11} = 0.66$, ns]. *$P < 0.05$, ** $P < 0.01$, *** $P < 0.001$, ns: non-significant.

**Fig. 4. Evidence for LI-rTMS-induced APs.**

**(A)** Comparison of spontaneous and LI-rTMS-induced APs. **(Aa)** Intracellular activity recorded from an S1 pyramidal neuron in control and during LI-rTMS, before (with artifacts, vertical red lines) and after (without artifacts) removal of stimulation artifacts. Here and in the following panels, open stars mark the occurrence of spontaneous (black) and putative LI-rTMS-evoked (red) APs. A typical example of a putative LI-rTMS-evoked AP, with and without artifact, is enlarged above the records. Note that the depolarizing phase of the LI-rTMS-evoked AP is hidden within the artifact. **(Ab)** *S*uperimposition of 3 spontaneous (black) or LI-rTMS-induced (red) APs (light-colored traces) with their corresponding average waveform (deeper-colored traces). The AP amplitude is normalized and LI-rTMS artifacts are indicated by dotted red lines. Note the similarity in the repolarization phase of spontaneous and LI-rTMS-induced APs when average waveforms are merged (right). The insets show the corresponding AP phase-plots (with only the repolarization phase illustrated for LI-rTMS induced APs). **(B)** Spontaneous and LI-rTMS-induced APs are blocked by membrane hyperpolarization. Intracellular activity of an S1 cortical neuron in absence of (Control, top traces) and during LI-rTMS (bottom traces) at rest (left panel) and during membrane hyperpolarization induced by intracellular injection of negative *DC*-current (middle and right panels). Red vertical markers above the traces indicate the position of the removed artifacts. **(C)** AP blockade by QX-314 in control and during LI-rTMS. **(Ca)** Examples of intracellular records obtained in absence of (left) and during (right) LI-rTMS at the indicated times after impalement with a microelectrode containing 100 mM QX-314. Times after impalement are indicated between each set of traces. Note the progressive decrease in the amplitude of both spontaneous and LI-rTMS-triggered APs, which start to resemble sharp synaptic depolarizations at 30 and 40 min after onset of QX-314 diffusion (arrows). **(Cb)** Changes in peak potential value of individual spontaneous (black), LI-rTMS-induced (red) and current-induced (gray) APs in an S1 neuron, as a function of time after onset of QX-314 diffusion. The peak value of the first AP in each group, measured just after cell impalement, was taken as reference and artificially set to zero mV. Insets show representative current-evoked responses at the indicated times after cell impalement are shown on top. **(Cc)** Pooled data comparing the peak potential decrease of spontaneous (black), LI-rTMS-induced (red) and current-induced (gray) APs at different times after QX-314 diffusion onset. [Mixed Effects ANOVA; Spont: $n$ = 7, 5, 5 neurons; LI-rTMS-induced: $n$ = 8, 5, 5 neurons; Current-induced: $n$ = 8, 6, 5.

Effect of time, $F_{1.21,\ 9,72} = 16,64$, $P = 0.0017$; Effect of stimulation, $F_{1.33,\ 10,64} = 20.13$ $P = 0.0006$). Between groups ANOVA: t0, $F_{2,\ 24} = 2.34$; t10, $F_{2,\ 20} = 1.56$; t15-20, $F_{2,\ 13} = 0.68$; t30-40, $F_{2,\ 12} = 1.81$. At each time-point, all comparisons, ns]. ns: non-significant.

**Fig. 5. Changes in firing rate during LI-rTMS.**

**(A)** Intracellular activity of a representative active (Cell 1, located in layer 2/3) and a representative silent (Cell 2, located in layer 5) cortical neuron recorded before (Pre) and during LI-rTMS after artifacts removal. Neuronal firing increases markedly during the stimulation period. **(B)** Time course of the mean (± SD, $n$ = 16 neurons) changes in global firing frequency (including both spontaneous and LI-rTMS-induced APs; left) and of the specific rate of spontaneous (blue line) and TMS-mediated (red line) APs (right), calculated over 30-second periods before and during LI-rTMS (red arrow). **(C)** Summary plot comparing the mean (± SD) total AP frequency in Pre and LI-rTMS periods, separating cells that were active (black circles) and silent (gray circles) during baseline. [$n$ = 8 active and 7 silent neurons, Wilcoxon Signed Rank test, *$P < 0.05$].

**Fig. 6. Repetitive current-evoked firing in cortical neurons does not reproduce LI-rTMS effects**

**(A)** Intracellular activity of a representative S1 neuron before, during and after application of repetitive current pulse stimulation (rCPS). The rCPS protocol consisted of injecting a series of depolarizing current pulses (0.2 nA, 40 ms duration) at 10 Hz for 10 min (lower trace). **(B)** Comparison of neuronal firing during rCPS and LI-rTMS protocols. Left, Examples of short periods of intracellular activity recorded during LI-rTMS (top trace) and rCPS (bottom trace) paradigms. The onset time of the removed LI-rTMS artifacts is indicated by the red vertical markers and the timing of depolarizing current pulses is shown below the bottom trace. Middle, Pooled data comparing the mean (± SD) number of APs/stim. evoked by LI-rTMS or current pulses, and the total number of APs (evoked and spontaneous) measured over the whole stimulation period in response to rCPS ($n$ = 7 neurons, orange triangles) or LI-rTMS ($n$ = 9 neurons, red triangles) are shown at right. Right, Time course of the mean change (solid lines, $n$ = 7 neurons) ± SD (shaded areas) in AP frequency (after subtraction of the mean Pre value) calculated over successive 30-second periods, before and during rCPS (orange) or LI-rTMS (red) protocols. Dotted line indicates the mean Pre value, artificially set to zero. **(C)** Summary data comparing the changes in Vm, σVm, Rm, τm, γ and Ith values between pre- and post-stimulation periods after application of rCPS (orange circles) or LI-rTMS (blue circles) protocols. Dashed lines indicate the mean pre-stimulation value (Pre), artificially set to zero [Vm: $n$ = 7, 8; σVm: $n$ = 7, 9, Rm: $n$ = 7, 6; γ: $n$ = 7, 6; Ith: $n$ = 7, 6; unpaired Student t-test; and τm: $n$ = 7, 6; Mann Whitney Rank Sum test; ** $P < 0.01$, *** $P < 0.001$, ns: non-significant].

## Materials and Methods

### Study design

#### *Research objectives and experimental design*

This controlled laboratory study aimed to identify *in vivo* the acute effects of LI-rTMS on single identified neocortical neurons, which could explain the long-term changes in brain function induced by weak magnetic fields. Care and manipulation of animals were carried out in accordance with the guidelines of the European Union (directive 2010/603/EU), and received approval (APAFIS no. 18003-2019051019017280) from the French Ministry for Research and the *Charles Darwin* Ethical Committee on Animal Experimentation (C2EA-05). After completion of the surgical procedures under deep anesthesia, ECoG and intracellular recordings form S1 pyramidal neurons were performed on animals sedated with sufentanil. Sedation with sufentanil (*58*) was chosen because it induces a globally stable background ECoG activity characterized by low amplitude desynchronized cortical waves resembling those encountered during the waking state (*22*, *23*, *31*, *32*, *59*). It thus avoids anesthesia-related modulation of cortical responses to magnetic stimulation, as observed in both animal and human studies (*3*, *19*, *30*). Physiological parameters were continuously controlled during the long process of stimulation and recording. Each animal formed its own control, with LI-rTMS effects being compared to baseline measurements obtained before the start of magnetic stimulations.

#### *Sample size*

Sample size was determined on the basis of our previous experience with the number of recorded neurons necessary to demonstrate real biological effects during prolonged recordings *in vivo*. The exact number of neurons and animals used in each experimental group are indicated in the text or in the figure legends.

522 ***Data inclusion/exclusion criteria***

523 Animals whose baseline physiological parameters were outside the range of normal values
524 for rodents (*60*) were not included in the data set. This represented less than 5% of rats.
525 Cortical neurons that did not show stable electrical membrane properties during baseline
526 periods were excluded from the analysis. All quantitative analysis of data was performed
527 identically in each experimental group using objective measurements.

528 ***Outliers***

529 Potential outliers ($n \leq 2$ neurons in each experimental group) were identified in GraphPad
530 Prism 9.0, using the ROUT method with Q set to 1% (*i.e.*, less than 1% of detected outliers
531 would be in error).

532

533 **Animals, their preparation and surgery**

534

535 Experiments were conducted *in vivo* on adult Sprague Dawley rats ($n$ = 31) of both sexes
536 (Charles River Laboratories, France). Animals were first anesthetized by inhalation of
537 isoflurane (3.5%; Centravet, France) and underwent tracheotomy for artificial ventilation
538 (room air, 85 breaths.min$^{-1}$, 2.6 ml.cycle$^{-1}$) under neuromuscular blockade (gallamine
539 triethiodide, 40 mg/2h i.m; Sigma-Aldrich, France). They were placed in a stereotaxic frame
540 and small craniotomies were made above the left barrel field of S1 (1.2–1.3 mm posterior
541 to bregma, 4.1–6.5 mm lateral to midline; (*61*) to allow simultaneous recording of ECoG
542 and intracellular activity of subjacent pyramidal neurons. After craniotomy, isoflurane was
543 discontinued, but sedation and analgesia were maintained by repeated injection of sufentanil
544 (3 µg/kg every 30 min, i.p.; Piramal) and local infiltration of lidocaine (2%, Centravet) in
545 incision and pressure points. Heart rate and ECoG activity were continuously monitored to
546 assess the depth of sedation, and we ensured the stability of physiological parameters, i.e.

647 end-tidal carbon dioxide concentration ($EtCO_2$), oxygen saturation ($SpO_2$) and core
648 temperature (37°C) throughout the experiments (*23*, *62*). At the end of recordings, animals
649 were euthanized with an overdose of euthasol (40%, i.p.; Centravet) for subsequent
650 histological examination.
651
652 ***In vivo* multi-scale electrophysiological recordings**
653 Intracellular recordings were performed with glass micropipettes filled with 2-M potassium
654 acetate (50-90 MΩ). Current-clamp recordings were amplified using an Axoclamp 900A
655 amplifier (Molecular Devices, Union City, CA, USA) operating in bridge mode, filtered
656 between *DC* and 30 KHz and digitized at 10 kHz (CED 1401plus, Spike2 software version
657 7.06; Cambridge Electronic Design). Intracellularly recorded neurons ($n$ = 41), identified
658 as pyramidal cells by their morphological and electrophysiological characteristics (*63*),
659 were located in layers 2/3 and 5 at depths ranging between 800–3300 µm below the cortical
660 surface (*61*, *64*). In a subset of experiments ($n$ = 8), we added to the pipette solution 50–
661 100 mM of N-2.6-dimethyl-phenyl carbamoyl methyl triethyl ammonium bromide (QX-
662 314; Tocris Biosciences), a voltage-gated sodium channels blocker known to suppress APs
663 in a time-dependent manner (*28*, *65*).
664 Spontaneous ECoG activity was recorded by means of a low impedance (~60 kΩ)
665 silver electrode placed on the dura above S1 and a reference electrode placed on a
666 contralateral temporal muscle. Surface cortical signals were amplified using a differential
667 *AC* amplifier (Model 1700; A-M Systems), filtered at 1 Hz–1 kHz, and digitized at 3 kHz.
668
669 **Stimulation protocols**
670 Stimulated animals received a single session LI-rTMS applied at 10 Hz for 10 minutes (6000
671 pulses). Magnetic pulses were delivered using a custom-designed miniaturized round coil

572 connected to an electromagnetic pulse generator (E-Lab5, Global Energy Medicine, Perth,
573 Australia). The coil (copper wire: 0.25-mm, 16 Ω, 300 turns) was suitable for use in rodents,
574 with an 8-mm outer diameter and a central 5-mm diameter steel core to increase field
575 penetration into the brain (*13*). The coil was secured to a micromanipulator and placed above
576 S1 at the center of the craniotomy (Fig. 1A). Brain-to-coil distance was kept minimal (~2
577 mm) while assuring contact-free stimulation and the coil orientation was adjusted to be
578 tangential to the surface of S1. The non-sinusoidal 300-µs monophasic magnetic pulses had
579 a 230-µs rise time and generated a field of 10 mT, without sound, vibration, or heat above
580 background, as previously described (*12*, *13*). We also verified that LI-rTMS did not cause
581 electromagnetic interference in the recording leads and electrodes in negative control
582 experiments in which a model cell (CLAMP-1U Model Cell, Molecular Devices, Union
583 City, CA, USA) in 'cell mode' was attached to the headstage amplifier (fig. S2B).

584 Repetitive current pulse stimulation (rCPS) consisted of the intracellular injection
585 of depolarizing square current pulses (40 ms of duration) at 10 Hz for 10 min. The intensity
586 of the current pulses (0.1–0.5 nA) was adjusted for each neuron to evoke an AP every 3–5
587 current pulses in order to mimic the frequency of LI-rTMS-induced APs.

588

589 **Intracellular and ECoG signals analysis**

590 Spontaneous activity, membrane excitability and integrative properties of cortical
591 neurons were assessed before and after LI-rTMS. Average membrane potential (Vm) was
592 calculated as the mean of the distribution of spontaneous subthreshold membrane potential
593 values and the magnitude of Vm fluctuations was quantified as the standard deviation (σ)
594 of the distribution (σVm). Time-frequency maps illustrating the spectral content of synaptic
595 activity over time were constructed using a multitaper decomposition analysis with a sliding
596 time window of 3 seconds (*66*), after the removing of APs which were replaced by a

piecewise cubic hermite polynomial interpolation. Power spectra were computed by averaging the time-frequency decomposition over a 10-minute period.

Mean spontaneous firing rate and Vm values were measured from recordings of at least 1 min. The regularity of neuronal firing was calculated by the CV2 method: here CV2 = $(2|\Delta t_{i+1} - \Delta t_i|)/(\Delta t_{i+1} + \Delta t_i)$, and $\Delta t_i = t_i - t_{i-1}$ is the inter-spike-interval (*22*). AP properties were measured from spontaneously occurring APs. AP voltage threshold was defined as the Vm at which $dVm.dt^{-1}$ first exceeds 10 $mV.ms^{-1}$ (*21*). AP amplitude was calculated from threshold to peak potential and AP half-width was the duration of the waveform at half-amplitude.

Dynamic changes of Vm, σVm and spontaneous firing frequency were assessed over successive windows of 30 seconds. Recording periods during which cortical excitability was assessed (see below) were removed from this analysis and replaced by a linear interpolation.

Rm was calculated as the slope of the linear portion of voltage-current (*V-I*) plots generated following repeated injections of hyperpolarizing current of increasing intensity (200 ms at 2 Hz, 10–20 trials per intensity, -0.2 to -0.8 nA) or from the average voltage deflection induced by hyperpolarizing current pulses of -0.4 nA (200 ms, ≥ 10 trials). τm was derived from an exponential decay fit applied to the initial phase of the mean current-induced hyperpolarization. Neuronal transfer function (*F–I* relationship), which describes the cell output firing as a function of injected depolarizing current pulses of increasing intensity (200 ms at 2 Hz, 10–20 trials per intensity, 0.1–1.5 nA), was quantified before and after application of LI-rTMS. Linear regression of *F–I* curves yielded the threshold current for AP generation ($I_{th}$; *x*-intercept) and neuronal gain (γ; slope) (*21*, *22*).

**LI-rTMS artifact removal**

To assess changes in cortical activity *during* the 10 minutes of LI-rTMS, we removed brief high-amplitude electrical artifacts induced by the magnetic pulses by eliminating the recorded signal for a window of 1.6 ms following each pulse onset. Linear interpolation was used to preserve continuity (fig. S2). Similar approaches have been used to handle similar stimulation artifacts in combined TMS-EEG experiments in humans (*67–69*) or in intracranial current stimulation and recordings in implanted patients (*70*). We validated this approach, by adding a new channel containing artificially generated stimulation events at 10 Hz for 10 minutes to control recordings. These false artifacts were then removed with the same procedure and the resulting electrophysiological signal compared to the original to ensure their similarity (*70*).

**Neuronal labelling**

Cortical neurons were filled with neurobiotin (1.5% added to the pipette solution; Vector Laboratories, Burlingame, CA, USA) through repeated intracellular injections of depolarizing current pulses (0.2–1 nA; 100 ms) applied at 2–3 Hz for 10 minutes after the end of the post-stimulation period (*20*) (Mahon and Charpier, 2012). Rats were then rapidly euthanized with euthasol and transcardially perfused with 0.3% glutaraldehyde-4% paraformaldehyde in phosphate-buffered saline (0.1 M, pH 7.4; VWR Chemicals, France). The histochemical methods used to reveal the morphology of neurobiotin-filled neurons have been previously described in detail (*71*).

**Statistical analysis**

All data were explored for normality, outliers and fulfillment of statistical tests assumptions in Prism version 9.00 (GraphPad software Inc., San Diego, USA). Differences between groups were assessed using paired two-tailed Student's t-test, one-way Repeated Measures

ANOVA, or the non-parametric Wilcoxon signed rank test and the Mann-Whitney rank sum test when appropriate. The sequential rejective Benjamini-Hochberg test procedure was used to correct for multiple comparisons (*72*). All values are expressed as means ± SD and significance level was set at $P < 0.05$.

## References


1. G. S. Pell, Y. Roth, A. Zangen, Modulation of cortical excitability induced by repetitive transcranial magnetic stimulation: influence of timing and geometrical parameters and underlying mechanisms. *Prog. Neurobiol.* **93**, 59–98 (2011).

2. P. M. Rossini, D. Burke, R. Chen, L. G. Cohen, Z. Daskalakis, R. Di Iorio, V. Di Lazzaro, F. Ferreri, P. B. Fitzgerald, M. S. George, M. Hallett, J. P. Lefaucheur, B. Langguth, H. Matsumoto, C. Miniussi, M. A. Nitsche, A. Pascual-Leone, W. Paulus, S. Rossi, J. C. Rothwell, H. R. Siebner, Y. Ugawa, V. Walsh, U. Ziemann, Non-invasive electrical and magnetic stimulation of the brain, spinal cord, roots and peripheral nerves: Basic principles and procedures for routine clinical and research application. An updated report from an I.F.C.N. Committee. *Clin. Neurophysiol.* **126**, 1071–1107 (2015).

3. H. R. Siebner, G. Hartwigsen, T. Kassuba, J. C. Rothwell, How does transcranial magnetic stimulation modify neuronal activity in the brain? Implications for studies of cognition. *Cortex J.* **45**, 1035–1042 (2009).

4. T. Wagner, J. Rushmore, U. Eden, A. Valero-Cabre, Biophysical foundations underlying TMS: setting the stage for an effective use of neurostimulation in the cognitive neurosciences. *Cortex J.* **45**, 1025–1034 (2009).

5. A. Vlachos, F. Müller-Dahlhaus, J. Rosskopp, M. Lenz, U. Ziemann, T. Deller, Repetitive magnetic stimulation induces functional and structural plasticity of excitatory postsynapses in mouse organotypic hippocampal slice cultures. *J. Neurosci.* **32**, 17514–17523 (2012).

6. M. Lenz, C. Galanis, F. Müller-Dahlhaus, A. Opitz, C. J. Wierenga, G. Szabó, U. Ziemann, T. Deller, K. Funke, A. Vlachos, Repetitive magnetic stimulation induces plasticity of inhibitory synapses. *Nat. Commun.* **7**, 10020 (2016).

7. A. Mix, K. Hoppenrath, K. Funke, Reduction in cortical parvalbumin expression due to intermittent theta-burst stimulation correlates with maturation of the perineuronal nets in young rats. *Dev. Neurobiol.* **75**, 1–11 (2015).

8. K. Hoppenrath, W. Härtig, K. Funke, Intermittent Theta-Burst Transcranial Magnetic Stimulation Alters Electrical Properties of Fast-Spiking Neocortical Interneurons in an Age-Dependent Fashion. *Front. Neural Circuits*. **10**, 22 (2016).

9. C. M. Cook, D. M. Saucier, A. W. Thomas, F. S. Prato, Changes in human EEG alpha activity following exposure to two different pulsed magnetic field sequences. *Bioelectromagnetics*. **30**, 9–20 (2009).

10. V. Di Lazzaro, F. Capone, F. Apollonio, P. A. Borea, R. Cadossi, L. Fassina, C. Grassi, M. Liberti, A. Paffi, M. Parazzini, K. Varani, P. Ravazzani, A consensus panel review of central nervous system effects of the exposure to low-intensity extremely low-frequency magnetic fields. *Brain Stimulat.* **6**, 469–476 (2013).

11. M. L. Rohan, R. T. Yamamoto, C. T. Ravichandran, K. R. Cayetano, O. G. Morales, D. P. Olson, G. Vitaliano, S. M. Paul, B. M. Cohen, Rapid mood-elevating effects of low field magnetic stimulation in depression. *Biol. Psychiatry*. **76**, 186–193 (2014).

12. J. Rodger, C. Mo, T. Wilks, S. A. Dunlop, R. M. Sherrard, Transcranial pulsed magnetic field stimulation facilitates reorganization of abnormal neural circuits and corrects behavioral deficits without disrupting normal connectivity. *FASEB J.* **26**, 1593–1606 (2012).

13. K. Makowiecki, A. R. Harvey, R. M. Sherrard, J. Rodger, Low-intensity repetitive transcranial magnetic stimulation improves abnormal visual cortical circuit topography and upregulates BDNF in mice. *J. Neurosci.* **34**, 10780–10792 (2014).

14. T. Dufor, S. Grehl, A. D. Tang, M. Doulazmi, M. Traoré, N. Debray, C. Dubacq, Z.-D. Deng, J. Mariani, A. M. Lohof, Neural circuit repair by low-intensity magnetic stimulation requires cellular magnetoreceptors and specific stimulation patterns. *Sci. Adv.* **5**, eaav9847 (2019).

15. S. Grehl, H. M. Viola, P. I. Fuller-Carter, K. W. Carter, S. A. Dunlop, L. C. Hool, R. M. Sherrard, J. Rodger, Cellular and molecular changes to cortical neurons following low intensity repetitive magnetic stimulation at different frequencies. *Brain Stimulat.* **8**, 114–123 (2015).

16. C. Y. Chan, C. Nicholson, Modulation by applied electric fields of Purkinje and stellate cell activity in the isolated turtle cerebellum. *J. Physiol.* **371**, 89–114 (1986).

17. T. Radman, R. L. Ramos, J. C. Brumberg, M. Bikson, Role of cortical cell type and morphology in subthreshold and suprathreshold uniform electric field stimulation in vitro. *Brain Stimulat.* **2**, 215–228, 228.e1–3 (2009).

18. S. Grehl, D. Martina, C. Goyenvalle, Z.-D. Deng, J. Rodger, R. M. Sherrard, In vitro Magnetic Stimulation: A Simple Stimulation Device to Deliver Defined Low Intensity Electromagnetic Fields. *Front. Neural Circuits*. **10**, 85 (2016).

19. J. Silvanto, A. Pascual-Leone, State-dependency of transcranial magnetic stimulation. *Brain Topogr.* **21**, 1–10 (2008).

20. J. J. Zhu, B. W. Connors, Intrinsic firing patterns and whisker-evoked synaptic responses of neurons in the rat barrel cortex. *J. Neurophysiol.* **81**, 1171–1183 (1999).

21. S. Mahon, S. Charpier, Bidirectional plasticity of intrinsic excitability controls sensory inputs efficiency in layer 5 barrel cortex neurons in vivo. *J. Neurosci.* **32**, 11377–11389 (2012).

22. T. Altwegg-Boussac, M. Chavez, S. Mahon, S. Charpier, Excitability and responsiveness of rat barrel cortex neurons in the presence and absence of spontaneous synaptic activity in vivo. *J. Physiol.* **592**, 3577–3595 (2014).

23. T. Altwegg-Boussac, A. E. Schramm, J. Ballestero, F. Grosselin, M. Chavez, S. Lecas, M. Baulac, L. Naccache, S. Demeret, V. Navarro, S. Mahon, S. Charpier, Cortical neurons and networks are dormant but fully responsive during isoelectric brain state. *Brain J.* **140**, 2381–2398 (2017).

24. M. Brecht, A. Roth, B. Sakmann, Dynamic receptive fields of reconstructed pyramidal cells in layers 3 and 2 of rat somatosensory barrel cortex. *J. Physiol.* **553**, 243–265 (2003).

25. I. D. Manns, B. Sakmann, M. Brecht, Sub- and suprathreshold receptive field properties of pyramidal neurones in layers 5A and 5B of rat somatosensory barrel cortex. *J. Physiol.* **556**, 601–622 (2004).

26. R. A. Silver, Neuronal arithmetic. *Nat. Rev. Neurosci.* **11**, 474–489 (2010).

27. A. D. Tang, I. Hong, L. J. Boddington, A. R. Garrett, S. Etherington, J. N. J. Reynolds, J. Rodger, Low-intensity repetitive magnetic stimulation lowers action potential threshold and increases spike firing in layer 5 pyramidal neurons in vitro. *Neuroscience*. **335**, 64–71 (2016).

28. B. W. Connors, D. A. Prince, Effects of local anesthetic QX-314 on the membrane properties of hippocampal pyramidal neurons. *J. Pharmacol.* **220**, 476–481 (1982).

29. L. S. Benardo, L. M. Masukawa, D. A. Prince, Electrophysiology of isolated hippocampal pyramidal dendrites. *J. Neurosci.* **2**, 1614–1622 (1982).

30. R. Gersner, E. Kravetz, J. Feil, G. Pell, A. Zangen, Long-term effects of repetitive transcranial magnetic stimulation on markers for neuroplasticity: differential outcomes in anesthetized and awake animals. *J. Neurosci.* **31**, 7521–7526 (2011).

31. R. M. Bruno, B. Sakmann, Cortex is driven by weak but synchronously active thalamocortical synapses. *Science*. **312**, 1622–1627 (2006).

32. C. M. Constantinople, R. M. Bruno, Effects and mechanisms of wakefulness on local cortical networks. *Neuron*. **69**, 1061–1068 (2011).

33. G. Bonmassar, S. W. Lee, D. K. Freeman, M. Polasek, S. I. Fried, J. T. Gale, Microscopic magnetic stimulation of neural tissue. *Nat. Commun.* **3**, 921 (2012).

34. J. Banerjee, M. E. Sorrell, P. A. Celnik, G. Pelled, Immediate Effects of Repetitive Magnetic Stimulation on Single Cortical Pyramidal Neurons. *PLoS ONE*. **12**, e0170528 (2017).

35. F. Müller-Dahlhaus, A. Vlachos, Unraveling the cellular and molecular mechanisms of repetitive magnetic stimulation. *Front. Mol. Neurosci.* **6**, 50 (2013).

36. T. Pashut, D. Magidov, H. Ben-Porat, S. Wolfus, A. Friedman, E. Perel, M. Lavidor, I. Bar-Gad, Y. Yeshurun, A. Korngreen, Patch-clamp recordings of rat neurons from acute

brain slices of the somatosensory cortex during magnetic stimulation. *Front. Cell. Neurosci.* **8**, 145 (2014).

37. J. C. Eccles, *The Physiology of Synapses* (Springer, Berlin, 1964).

38. M. H. P. Kole, S. U. Ilschner, B. M. Kampa, S. R. Williams, P. C. Ruben, G. J. Stuart, Action potential generation requires a high sodium channel density in the axon initial segment. *Nat. Neurosci.* **11**, 178–186 (2008).

39. A. Rotem, E. Moses, Magnetic stimulation of one-dimensional neuronal cultures. *Biophys. J.* **94**, 5065–5078 (2008).

40. B. N. Pasley, E. A. Allen, R. D. Freeman, State-dependent variability of neuronal responses to transcranial magnetic stimulation of the visual cortex. *Neuron*. **62**, 291–303 (2009).

41. D. Rudiak, E. Marg, Finding the depth of magnetic brain stimulation: a re-evaluation. *Electroencephalogr. Clin. Neurophysiol.* **93**, 358–371 (1994).

42. A. Destexhe, M. Rudolph, D. Paré, The high-conductance state of neocortical neurons in vivo. *Nat. Rev. Neurosci.* **4**, 739–751 (2003).

43. A. Carton-Leclercq, S. Lecas, M. Chavez, S. Charpier, S. Mahon, Neuronal excitability and sensory responsiveness in the thalamo-cortical network in a novel rat model of isoelectric brain state. *J. Physiol.* **599**, 609–629 (2021).

44. R. Tremblay, S. Lee, B. Rudy, GABAergic Interneurons in the Neocortex: From Cellular Properties to Circuits. *Neuron*. **91**, 260–292 (2016).

45. J. Xu, J. Kang, The mechanisms and functions of activity-dependent long-term potentiation of intrinsic excitability. *Rev. Neurosci.* **16**, 311–323 (2005).

46. B. Delord, H. Berry, E. Guigon, S. Genet, A New Principle for Information Storage in an Enzymatic Pathway Model. *PLOS Comput. Biol.* **3**, e124 (2007).

47. J. Naudé, J. T. Paz, H. Berry, B. Delord, A Theory of Rate Coding Control by Intrinsic Plasticity Effects. *PLOS Comput. Biol.* **8**, e1002349 (2012).

48. J. Lombardo, J. Sun, M. A. Harrington, Rapid activity-dependent modulation of the intrinsic excitability through up-regulation of KCNQ/Kv7 channel function in neonatal spinal motoneurons. *PLoS ONE*. **13**, e0193948 (2018).

49. C. Li, J. Lu, C. Wu, S. Duan, M. Poo, Bidirectional modification of presynaptic neuronal excitability accompanying spike timing-dependent synaptic plasticity. *Neuron*. **41**, 257–268 (2004).

50. R. M. Sherrard, N. Morellini, N. Jourdan, M. El-Esawi, L.-D. Arthaut, C. Niessner, F. Rouyer, A. Klarsfeld, M. Doulazmi, J. Witczak, A. d'Harlingue, J. Mariani, I. Mclure, C. F. Martino, M. Ahmad, Low-intensity electromagnetic fields induce human cryptochrome to modulate intracellular reactive oxygen species. *PLoS Biol.* **16**, e2006229 (2018).

51. A. Görlach, K. Bertram, S. Hudecova, O. Krizanova, Calcium and ROS: A mutual interplay. *Redox Biol.* **6**, 260–271 (2015).

52. Y.-Z. Huang, M. J. Edwards, E. Rounis, K. P. Bhatia, J. C. Rothwell, Theta burst stimulation of the human motor cortex. *Neuron*. **45**, 201–206 (2005).

53. G. Cirillo, G. Di Pino, F. Capone, F. Ranieri, L. Florio, V. Todisco, G. Tedeschi, K. Funke, V. Di Lazzaro, Neurobiological after-effects of non-invasive brain stimulation. *Brain Stimulat.* **10**, 1–18 (2017).

54. A. Bhattacharya, K. Mrudula, S. S. Sreepada, T. N. Sathyaprabha, P. K. Pal, R. Chen, K. Udupa, An Overview of Noninvasive Brain Stimulation: Basic Principles and Clinical Applications. *Can. J. Neurol.*, 1–14 (2021).

55. M. Lenz, S. Platschek, V. Priesemann, D. Becker, L. M. Willems, U. Ziemann, T. Deller, F. Müller-Dahlhaus, P. Jedlicka, A. Vlachos, Repetitive magnetic stimulation induces plasticity of excitatory postsynapses on proximal dendrites of cultured mouse CA1 pyramidal neurons. Brain Struct. Funct. 220, 3323–3337 (2015).

56. S. Mahon, J.-M. Deniau, S. Charpier, Corticostriatal plasticity: life after the depression. *Trends Neurosci.* **27**, 460–467 (2004).

57. V. K. Kimiskidis, A. Valentin, R. Kälviäinen, Transcranial magnetic stimulation for the diagnosis and treatment of epilepsy. *Curr. Opin. Neurol.* **27**, 236–241 (2014).

58. C. J. Niemegeers, K. H. Schellekens, W. F. Van Bever, P. A. Janssen, Sufentanil, a very potent and extremely safe intravenous morphine-like compound in mice, rats and dogs. *Arzneimittelforschung.* **26**, 1551–1556 (1976).

59. A. Depaulis, O. David, S. Charpier, The genetic absence epilepsy rat from Strasbourg as a model to decipher the neuronal and network mechanisms of generalized idiopathic epilepsies. *J. Neurosci. Methods*. **260**, 159–174 (2016).

60. S. Wolfensohn, Lloyd M, *Handbook of laboratory animal management and welfare*. (Blackwell Science, Oxford, 1998).

61. G. Paxinos, C. R. Watson, The Rat Brain in Stereotaxic Coordinates, *Acad. Press* (1986).

62. A. E. Schramm, A. Carton-Leclercq, S. Diallo, V. Navarro, M. Chavez, S. Mahon, S. Charpier, Identifying neuronal correlates of dying and resuscitation in a model of reversible brain anoxia. *Prog. Neurobiol.* **185**, 101733 (2020).

63. M. Steriade, Neocortical cell classes are flexible entities. *Nat. Rev. Neurosci.* **5**, 121–134 (2004).

64. W. B. Wilent, D. Contreras, Synaptic Responses to Whisker Deflections in Rat Barrel Cortex as a Function of Cortical Layer and Stimulus Intensity. *J. Neurosci.* **24**, 3985–3998 (2004).

65. C. J. Wilson, Y. Kawaguchi, The origins of two-state spontaneous membrane potential fluctuations of neostriatal spiny neurons. *J. Neurosci.* **16**, 2397–2410 (1996).

66. R. Oostenveld, P. Fries, E. Maris, J.-M. Schoffelen, FieldTrip: Open source software for advanced analysis of MEG, EEG, and invasive electrophysiological data. *Comput. Intell. Neurosci.* **2011**, 156869 (2011).

67. G. Thut, D. Veniero, V. Romei, C. Miniussi, P. Schyns, J. Gross, Rhythmic TMS causes local entrainment of natural oscillatory signatures. *Curr. Biol. CB*. **21**, 1176–1185 (2011).

68. M. Vernet, C. Stengel, R. Quentin, J. L. Amengual, A. Valero-Cabré, Entrainment of local synchrony reveals a causal role for high-beta right frontal oscillations in human visual consciousness. *Sci. Rep.* **9**, 14510 (2019).

69. C. Stengel, M. Vernet, J. L. Amengual, A. Valero-Cabré, Causal modulation of right hemisphere fronto-parietal phase synchrony with Transcranial Magnetic Stimulation during a conscious visual detection task. *Sci. Rep.* **11**, 3807 (2021).

70. J. L. Amengual, M. Vernet, C. Adam, A. Valero-Cabré, Local entrainment of oscillatory activity induced by direct brain stimulation in humans. *Sci. Rep.* **7**, 41908 (2017).

71. M. S. Williams, T. Altwegg-Boussac, M. Chavez, S. Lecas, S. Mahon, S. Charpier, Integrative properties and transfer function of cortical neurons initiating absence seizures in a rat genetic model. *J. Physiol.* **594**, 6733–6751 (2016).

72. Y. Benjamini, Y. Hochberg, Controlling the False Discovery Rate: A Practical and Powerful Approach to Multiple Testing. *J. R. Stat. Soc. Ser. B Methodol.* **57**, 289–300 (1995).

**Acknowledgments**

The authors thank Sarah Lecas for histological processing and all the technical staff from the Histomics core facility of the Paris Brain Institute.

**Funding:**

Agence nationale de la recherche, ANR-19-CE37-0021
Agence nationale de la recherche, ANR-10-IAIHU-06
Agence nationale de la recherche, # ANR-16-CE37-0021 2016
Fondation Recherche Alzheimer, (MB scholarship)

**Author contributions:**

Conceptualization: SM, RS, SC, AL, AVC
Methodology: MB, SM, SC, RS, AL, AVC
Investigation: MB
Data analysis: MB, PB, CS, SM, RS
Supervision: SM, RS, SC, AL, AVC
Writing – original draft: SM, SC, RS, AL

Writing – review & editing: SM, SC, RS, AL, MB, PB, AVC, CS

**Competing interests:** Authors declare that they have no competing interests.

**Data and materials availability:** All data are available in the main text or the supplementary materials.

## Figures and Tables

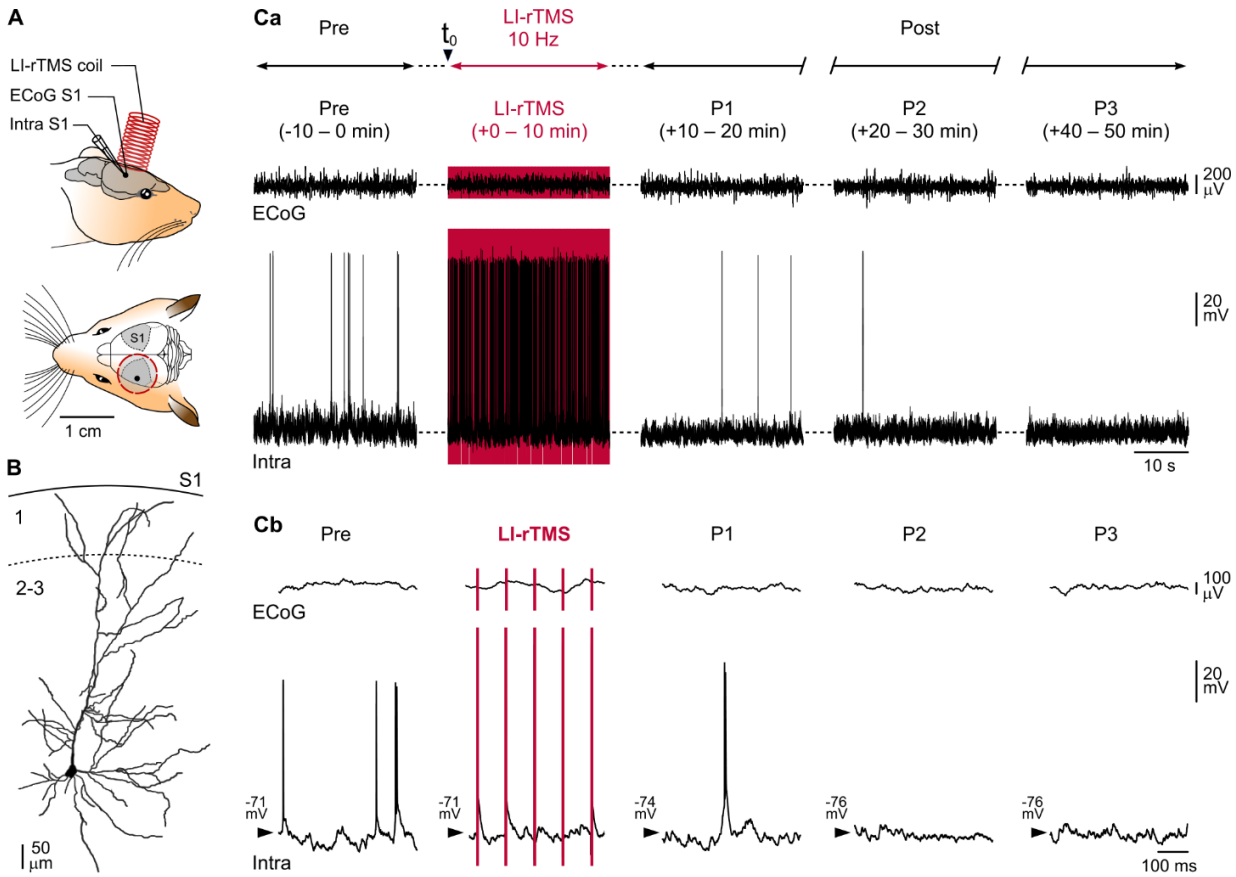


**Fig. 1. Experimental paradigm and definition of recording periods.**

(**A**) Schematic representation of the experimental set-up illustrating the positions of the LI-rTMS coil and the recording electrodes. ECoG activity from rat barrel cortex (S1) was monitored during intracellular recording of subjacent pyramidal neurons (Intra S1). LI-rTMS (10 Hz for 10 minutes) was delivered through a 8-mm wire coil placed ~2 mm away from the brain surface. **(B)** Reconstruction of a layer 2/3 pyramidal neuron filled with neurobiotin during recording. The dotted line indicates separation between cortical layers 1 and 2/3. **(Ca)** Simultaneous ECoG and intracellular recordings from a layer 2/3 pyramidal neuron, during the baseline period (Pre), the stimulation protocol (LI-rTMS), and at different times (+10−20 min, P1; +20−30 min, P2; +40−50 min, P3) after the onset of LI-rTMS (Post). **(Cb)** Expanded view (500 ms) of the recordings shown in **(Ca)**. The LI-rTMS

artifacts are shown in red. Here and in the following figures, the values of Vm are indicated at the left of intracellular records.

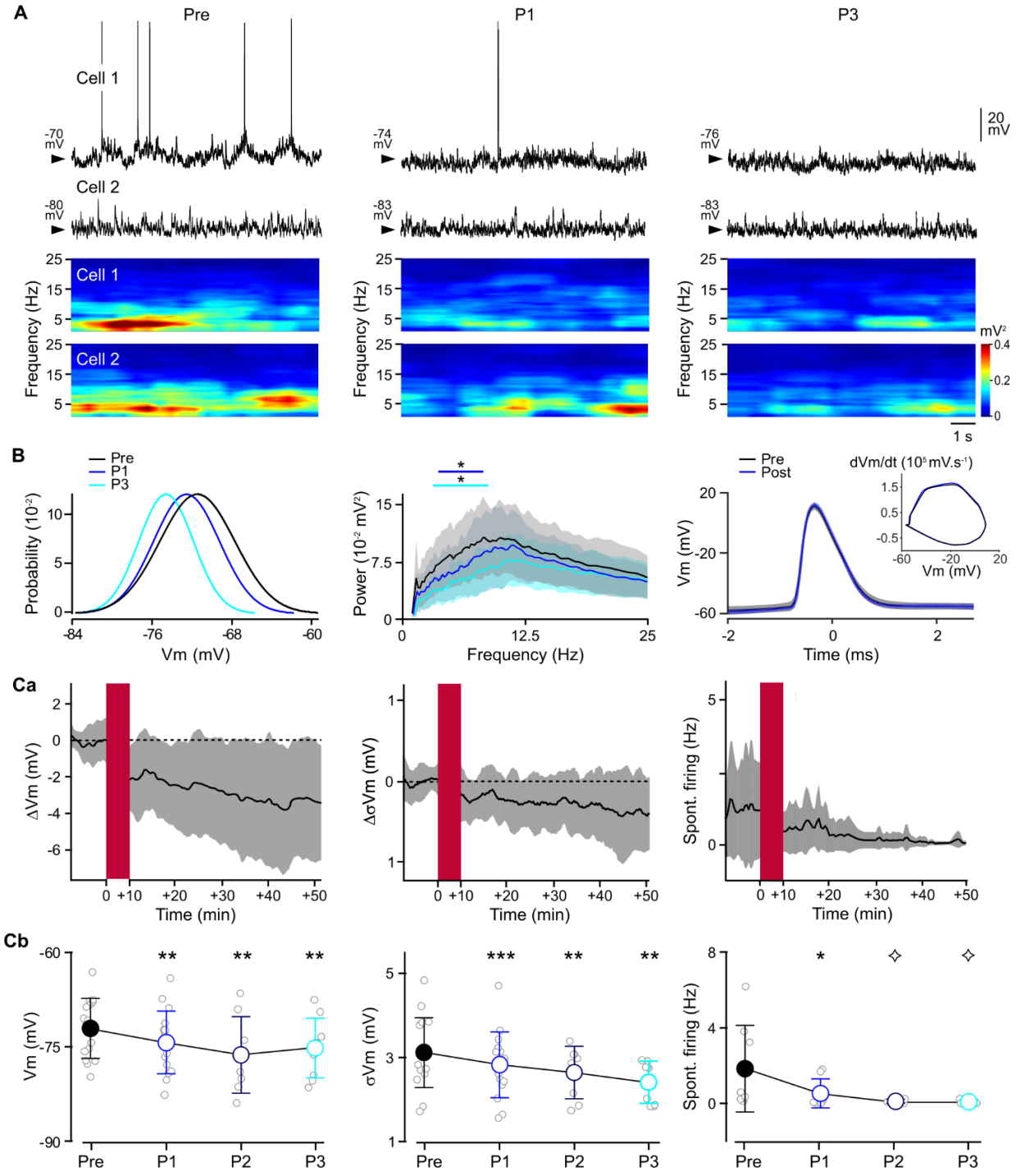


**Fig. 2. LI-rTMS causes lasting inhibition of cortical neurons spontaneous activity.** (**A**) Representative recordings of spontaneous intracellular activity of active (cell 1) and silent (cell 2) S1 neurons before LI-rTMS (Pre) and during the first (P1) and third (P3) post-stimulation periods. The associated time-frequency maps, after removal and interpolation

of APs, are temporally-aligned below the records. (**B**) Left: probability densities of Vm values computed from cell 2 during the different periods (60 sec of recording, bin size 1 mV). Middle: mean (solid lines) ± SD (shaded areas) frequency power spectra computed from intracellular subthreshold signals in the pre- and post-stimulation periods ($n$ = 16 neurons) showing a progressive decrease in the power of the 5-10 Hz frequency band after LI-rTMS (Wilcoxon signed rank test with Benjamini-Hochberg's post hoc correction, comparing P1 and P3 with Pre). Right: superimposed examples of average ± SD (shaded areas) of spontaneous APs and corresponding phase-plots (inset) during Pre (black trace, $n$ = 138) and Post (blue trace, $n$ = 28) LI-rTMS periods. **(C)** Time-dependent changes in cortical spontaneous activity after 10 minutes LI-rTMS. **(Ca)** Time course of the mean change (black line) ± SD (gray shaded area) in Vm (after subtraction of the mean Pre value), in the amplitude of Vm fluctuation (σVm; after subtraction of the mean Pre value), and in the spontaneous firing frequency of active neurons (Spont. Firing), calculated over successive 30-second periods before and after LI-rTMS application (red rectangle). **(Cb)** Comparison of Vm, σVm and spontaneous firing rate values (mean ± SD) during baseline (Pre) and at the three post-LI-rTMS periods (P1, P2, P3) [RMANOVA and Bonferroni post-hoc comparisons; Vm: $n$ = 16, 16, 8 and 9, $F_{0.39, 3.89} = 12.35$, $P = 0.034$; σVm: $n$ = 16, 16, 8 and 9, $F_{1.36, 13.55} = 11.69$, $P = 0.0025$; spontaneous firing: $n$ = 8, 8, 3 and 3, $F_{1.64, 6.03} = 9.74$, $P = 0.015$]. Here and in the following figures, the gray circles in the pooled-data graphs indicate values for individual neurons. In (Ca) and (Cb), analysis of ongoing firing was restricted to neurons which were spontaneously active during baseline. *$P < 0.05$, ** $P < 0.01$, *** $P < 0.001$, ns: non-significant; ◊ = too few data for post-hoc comparison.

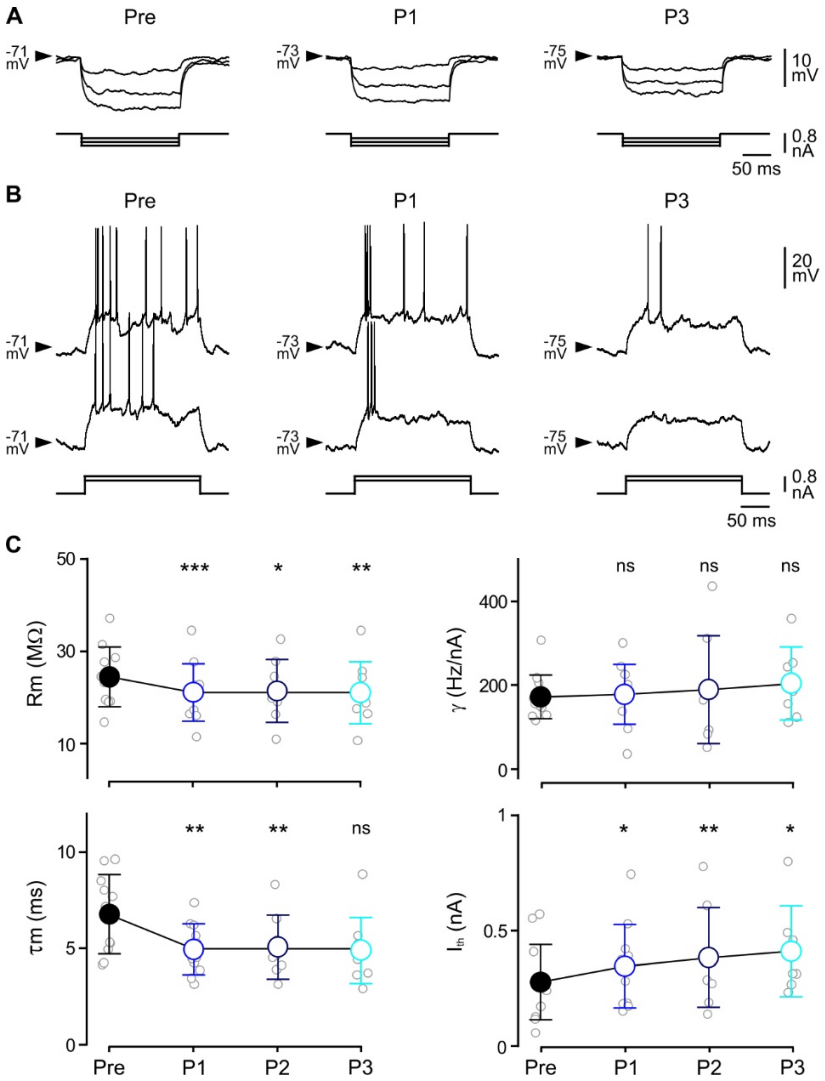


**Fig. 3. LI-rTMS negatively alters resting integrative properties and intrinsic excitability.**

(**A**) Average ($n$ = 6–30 trials) voltage responses (upper traces) of an S1 pyramidal neuron to hyperpolarizing current steps of increasing intensity (-0.2 to -0.6 nA, lower traces) before (Pre) and after LI-rTMS (periods P1 and P3). (**B**) Current-evoked firing responses to depolarizing current pulses of increasing intensity recorded from anS1 neuron in Pre, P1 and P3 periods. (**C**) Population data showing the temporal evolution of mean (± SD) values of Rm, τm, current threshold ($I_{th}$) and neuronal gain (γ) values. [RMANOVA and Bonferroni post-hoc comparisons; Rm: $n$ = 11, 11, 8 and 9, $F_{0.14, 1.19} = 10.54$, $P = 0.08$; τm: $n$ = 11, 11, 8 and 9, $F_{1.61, 13.44} = 8.24$, $P = 0.006$; $I_{th}$: $n$ = 12, 11, 8 and 7, $F_{0.72, 5.55} = 16.91$, $P = 0.01$; γ: $n$ = 12, 11, 8 and 7, $F_{0.14, 1.11} = 0.66$, ns]. *$P < 0.05$, ** $P < 0.01$, *** $P < 0.001$, ns: non-significant.

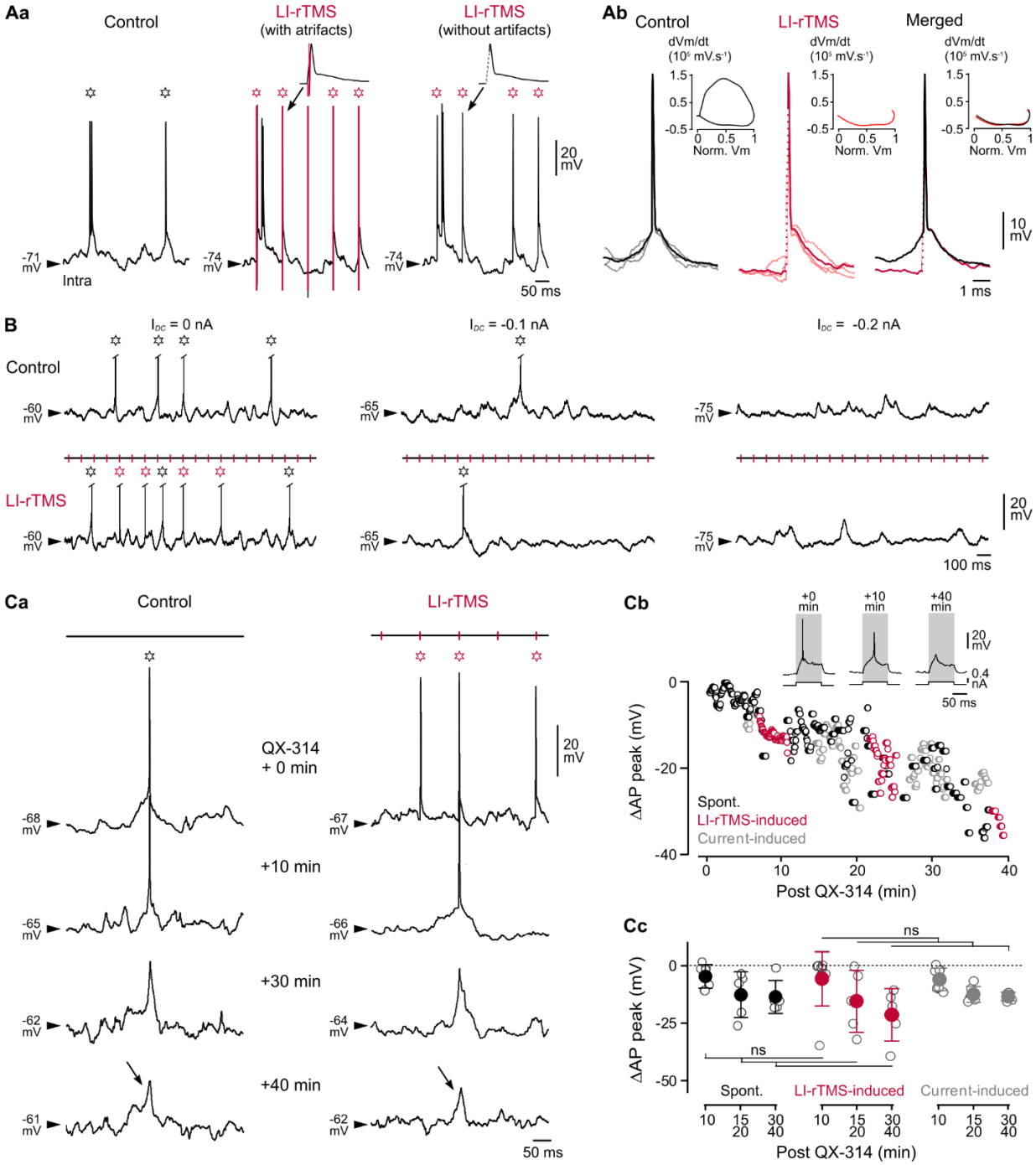


**Fig. 4. Evidence for LI-rTMS-induced APs.**

**(A)** Comparison of spontaneous and LI-rTMS-induced APs. **(Aa)** Intracellular activity recorded from an S1 pyramidal neuron in control and during LI-rTMS, before (with artifacts, vertical red lines) and after (without artifacts) removal of stimulation artifacts. Here and in the following panels, open stars mark the occurrence of spontaneous (black) and putative LI-rTMS-evoked (red) APs. A typical example of a putative LI-rTMS-evoked

AP, with and without artifact, is enlarged above the records. Note that the depolarizing phase of the LI-rTMS-evoked AP is hidden within the artifact. **(Ab)** *S*uperimposition of 3 spontaneous (black) or LI-rTMS-induced (red) APs (light-colored traces) with their corresponding average waveform (deeper-colored traces). The AP amplitude is normalized and LI-rTMS artifacts are indicated by dotted red lines. Note the similarity in the repolarization phase of spontaneous and LI-rTMS-induced APs when average waveforms are merged (right). The insets show the corresponding AP phase-plots (with only the repolarization phase illustrated for LI-rTMS induced APs). **(B)** Spontaneous and LI-rTMS-induced APs are blocked by membrane hyperpolarization. Intracellular activity of an S1 cortical neuron in absence of (Control, top traces) and during LI-rTMS (bottom traces) at rest (left panel) and during membrane hyperpolarization induced by intracellular injection of negative *DC*-current (middle and right panels). Red vertical markers above the traces indicate the position of the removed artifacts. **(C)** AP blockade by QX-314 in control and during LI-rTMS. **(Ca)** Examples of intracellular records obtained in absence of (left) and during (right) LI-rTMS at the indicated times after impalement with a microelectrode containing 100 mM QX-314. Times after impalement are indicated between each set of traces. Note the progressive decrease in the amplitude of both spontaneous and LI-rTMS-triggered APs, which start to resemble sharp synaptic depolarizations at 30 and 40 min after onset of QX-314 diffusion (arrows). **(Cb)** Changes in peak potential value of individual spontaneous (black), LI-rTMS-induced (red) and current-induced (gray) APs in an S1 neuron, as a function of time after onset of QX-314 diffusion. The peak value of the first AP in each group, measured just after cell impalement, was taken as reference and artificially set to zero mV. Insets show representative current-evoked responses at the indicated times after cell impalement are shown on top. **(Cc)** Pooled data comparing the peak potential decrease of spontaneous (black), LI-rTMS-induced (red) and current-induced (gray) APs at different times after QX-314 diffusion onset. [Mixed Effects ANOVA; Spont: $n$ = 7, 5, 5 neurons; LI-rTMS-induced: $n$ = 8, 5, 5 neurons; Current-induced: $n$ = 8, 6, 5. Effect of time, $F_{1.21,\ 9,72} = 16{,}64$, $P = 0.0017$; Effect of stimulation, $F_{1.33,\ 10,64} = 20.13$ $P = 0.0006$). Between groups ANOVA: t0, $F_{2,\ 24} = 2.34$; t10, $F_{2,\ 20} = 1.56$; t15-20, $F_{2,\ 13} = 0.68$; t30-40, $F_{2,\ 12} = 1.81$. At each time-point, all comparisons, ns]. ns: non-significant.

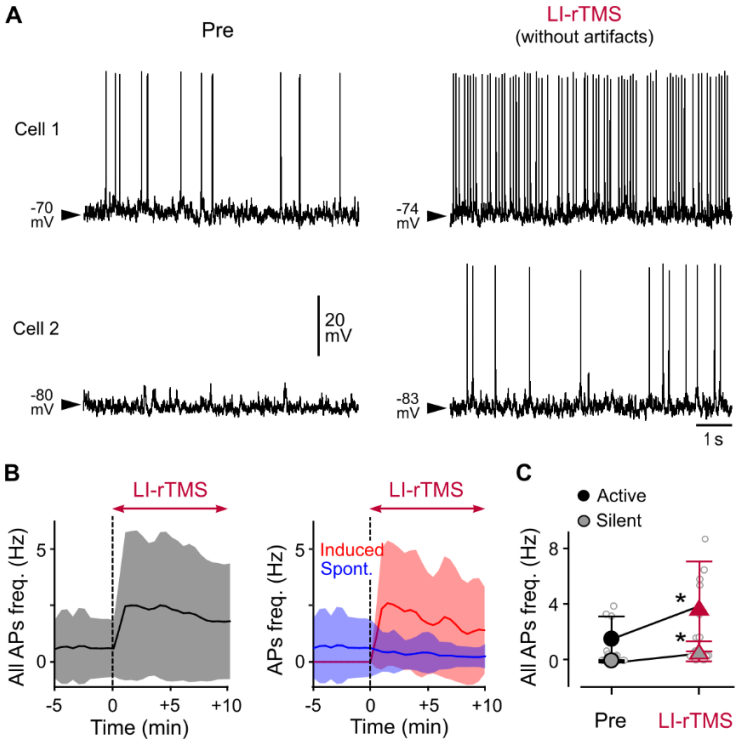


**Fig. 5. Changes in firing rate during LI-rTMS.**

**(A)** Intracellular activity of a representative active (Cell 1, located in layer 2/3) and a representative silent (Cell 2, located in layer 5) cortical neuron recorded before (Pre) and during LI-rTMS after artifacts removal. Neuronal firing increases markedly during the stimulation period. **(B)** Time course of the mean (± SD, $n$ = 16 neurons) changes in global firing frequency (including both spontaneous and LI-rTMS-induced APs; left) and of the specific rate of spontaneous (blue line) and TMS-mediated (red line) APs (right), calculated over 30-second periods before and during LI-rTMS (red arrow). **(C)** Summary plot comparing the mean (± SD) total AP frequency in Pre and LI-rTMS periods, separating cells that were active (black circles) and silent (gray circles) during baseline. [$n$ = 8 active and 7 silent neurons, Wilcoxon Signed Rank test, *$P < 0.05$].

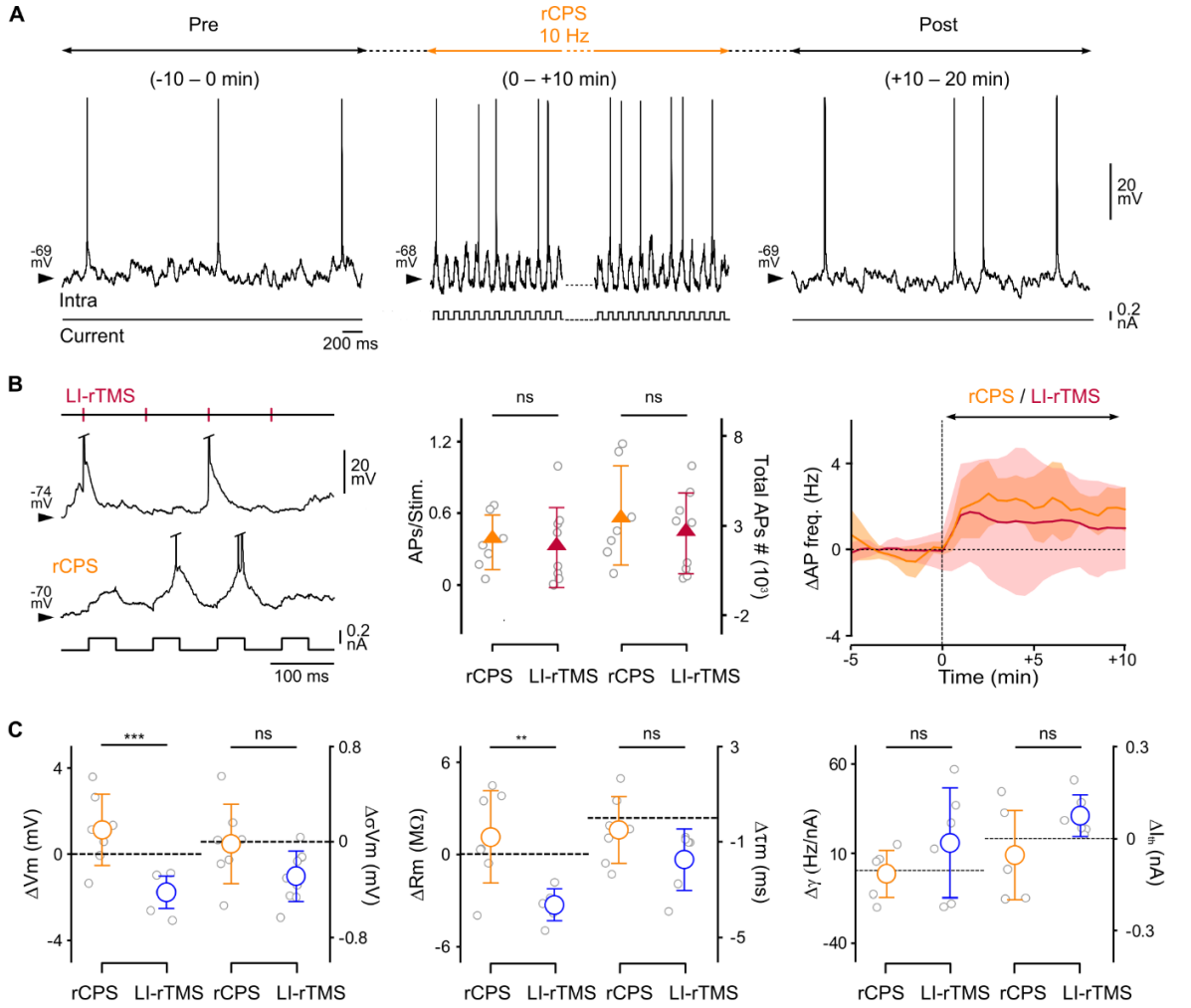


**Fig. 6. Repetitive current-evoked firing in cortical neurons does not reproduce LI-rTMS effects**

**(A)** Intracellular activity of a representative S1 neuron before, during and after application of repetitive current pulse stimulation (rCPS). The rCPS protocol consisted of injecting a series of depolarizing current pulses (0.2 nA, 40 ms duration) at 10 Hz for 10 min (lower trace). **(B)** Comparison of neuronal firing during rCPS and LI-rTMS protocols. Left, Examples of short periods of intracellular activity recorded during LI-rTMS (top trace) and rCPS (bottom trace) paradigms. The onset time of the removed LI-rTMS artifacts is indicated by the red vertical markers and the timing of depolarizing current pulses is shown below the bottom trace. Middle, Pooled data comparing the mean (± SD) number of APs/stim. evoked by LI-rTMS or current pulses, and the total number of APs (evoked and spontaneous) measured over the whole stimulation period in response to rCPS ($n$ = 7 neurons, orange triangles) or LI-rTMS ($n$ = 9 neurons, red triangles) are shown at right.

Right, Time course of the mean change (solid lines, $n$ = 7 neurons) ± SD (shaded areas) in AP frequency (after subtraction of the mean Pre value) calculated over successive 30-second periods, before and during rCPS (orange) or LI-rTMS (red) protocols. Dotted line indicates the mean Pre value, artificially set to zero. **(C)** Summary data comparing the changes in Vm, σVm, Rm, τm, γ and Ith values between pre- and post-stimulation periods after application of rCPS (orange circles) or LI-rTMS (blue circles) protocols. Dashed lines indicate the mean pre-stimulation value (Pre), artificially set to zero [Vm: $n$ = 7, 8; σVm: $n$ = 7, 9, Rm: $n$ = 7, 6; γ: $n$ = 7, 6; Ith: $n$ = 7, 6; unpaired Student t-test; and τm: $n$ = 7, 6; Mann Whitney Rank Sum test; ** $P < 0.01$, *** $P < 0.001$, ns: non-significant].

**Supplementary Materials**

Figures S1-S3
Table S1

# Supplementary Materials for

## *In vivo* low-intensity magnetic pulses durably alter neocortical neuron excitability and spontaneous activity

Manon Boyer, Paul Baudin, Chloé Stengel, Antoni Valero-Cabré, Ann Lohof, Stéphane Charpier, Rachel Sherrard*, Séverine Mahon

*Corresponding author: Rachel M Sherrard
Email: rachel.sherrard@sorbonne-universite.fr

**This PDF file includes:**

Figs. S1 to S3
Tables S1

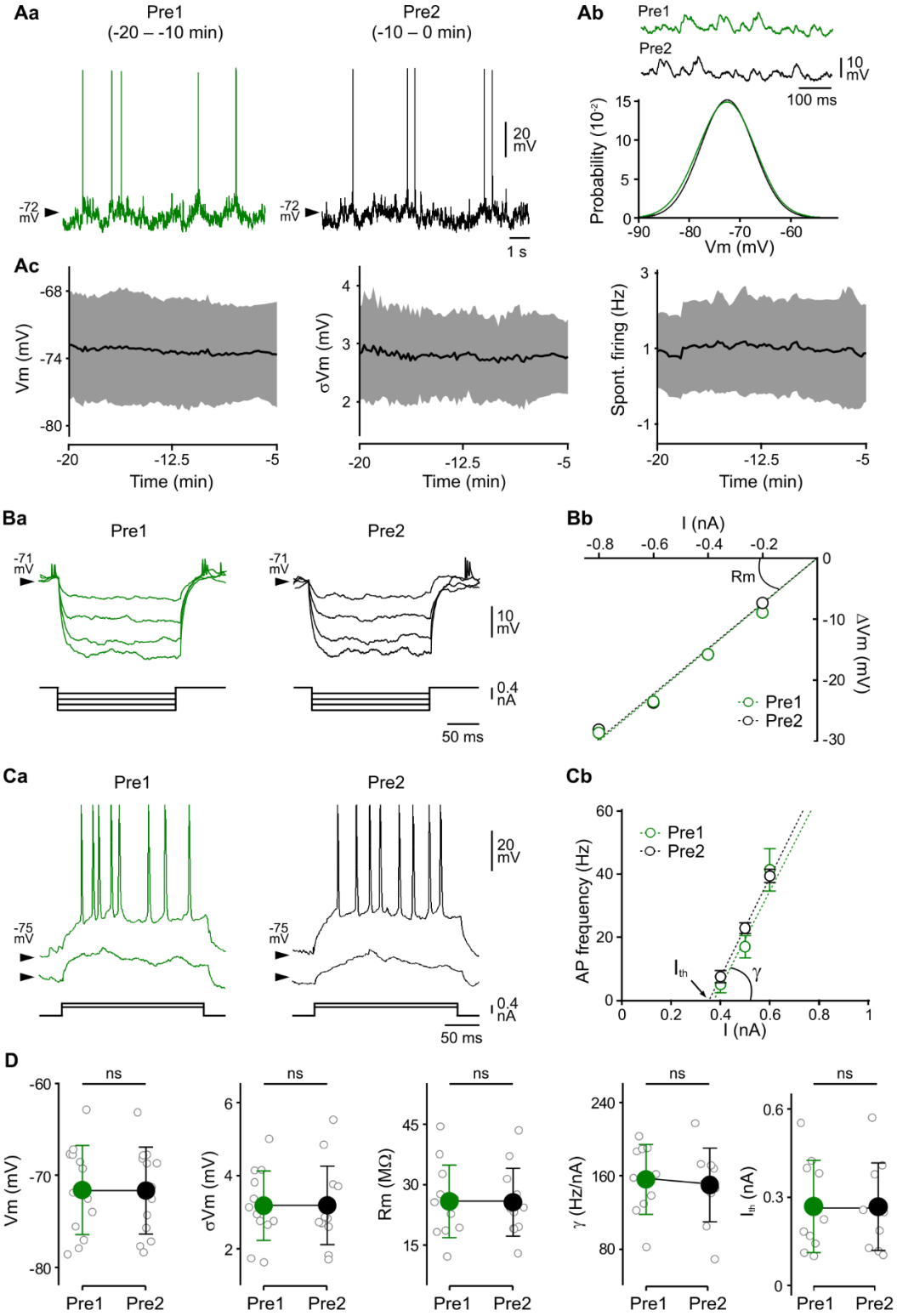
Aa
Pre1
(-20 – -10 min)
Pre2
(-10 – 0 min)
-72 mV
20 mV
1 s
Ab
Pre1
Pre2
10 mV
100 ms
Probability (10⁻²)
Vm (mV)
Ac
Vm (mV)
σVm (mV)
Spont. firing (Hz)
Time (min)
Ba
Pre1
Pre2
-71 mV
10 mV
0.4 nA
50 ms
Bb
I (nA)
Rm
ΔVm (mV)
Pre1
Pre2
Ca
Pre1
Pre2
-75 mV
20 mV
0.4 nA
50 ms
Cb
AP frequency (Hz)
I (nA)
Pre1
Pre2
γ
D
ns
Vm (mV)
σVm (mV)
Rm (MΩ)
γ (Hz/nA)
Pre1
Pre2

**Fig. S1. Stability of resting integrative properties and intrinsic excitability of cortical neurons over baseline periods.**

**(Aa)** Spontaneous intracellular activity of an S1 neuron recorded for two successive periods of 10 minutes: between 20–10 min (green trace, Pre1) and 10–0 min (black trace, Pre2) before the onset of the 10 min 10 Hz LI-rTMS protocol. Neuronal activity was characterized by a barrage of small-amplitude, broadband frequency, synaptic fluctuations (see also Fig. 2, A and B), confirming that sufentanil sedation induced cortical dynamics comparable to those observed during the waking state (*23*, *31, 32*). This background synaptic activity induced firing in 7 out of 13 neurons. Spontaneous firing rate of the active neurons was 2.9 ± 3.5 Hz during the first and 2.8 ± 3.5 Hz during the second pre-stimulation period (paired Student t-test, $P = 0.29$). Vm values are indicated at the left of intracellular records. **(Ab)** The probability densities of Vm values (60 s of recording, bin size 1 mV) demonstrate stability in the amplitude of synaptic activity over time. (Pre1 Vm = -71.6 ± 4.9 mV, $n = 13$ neurons *versus* Pre2 Vm, -71.7 ± 4.7 mV, $n = 13$ neurons; paired Student t-test, $P = 0.92$). **(Ac)** Time course of the mean values (solid lines, $n = 8$ neurons) ± SD (gray shaded areas) of Vm, σVm and spontaneous firing frequency computed over successive 30-second epochs during the 15 minutes of recording preceding LI-rTMS onset. Pearson's correlations indicate a lack of significant changes over time. **(B)** Stability of membrane input resistance. **(Ba)** Average ($n$ = 10–17 trials) voltage responses (top traces) to negative current pulses of increasing intensity (bottom traces) recorded from an S1 pyramidal neuron during the two baseline periods (green traces, Pre1 and black traces, Pre2). The corresponding *V–I* relationships shown in **(Bb)** were best fitted by linear regressions (dashed lines, both $r^2 > 0.99$), indicating a lack of substantial membrane rectification in the hyperpolarizing direction. **(C)** Constancy of cell intrinsic excitability over the pre-stimulation period. **(Ca)** Examples of current-induced firing responses to depolarizing current steps of increasing intensity recorded during the two successive baseline periods (green traces, Pre1; black traces, Pre2). **(Cb)** *F-I* relationships and corresponding linear fits for the neuron illustrated in **(Ca)**. Each data point is the mean (±SD) firing rate calculated from 10–18 successive trials. **(D)** Population data comparing Vm, σVm, Rm, γ and $I_{th}$ values during the two successive baseline periods. Gray circles correspond to values of individual neurons and green and black symbols show the mean ± SD. [Vm: $n = 13$; σVm: $n = 13$; Rm: $n = 12$; γ: $n = 10$; Ith: $n = 10$; paired Student t-test; *$P < 0.05$, *** $P < 0.001$, ns: non-significant].

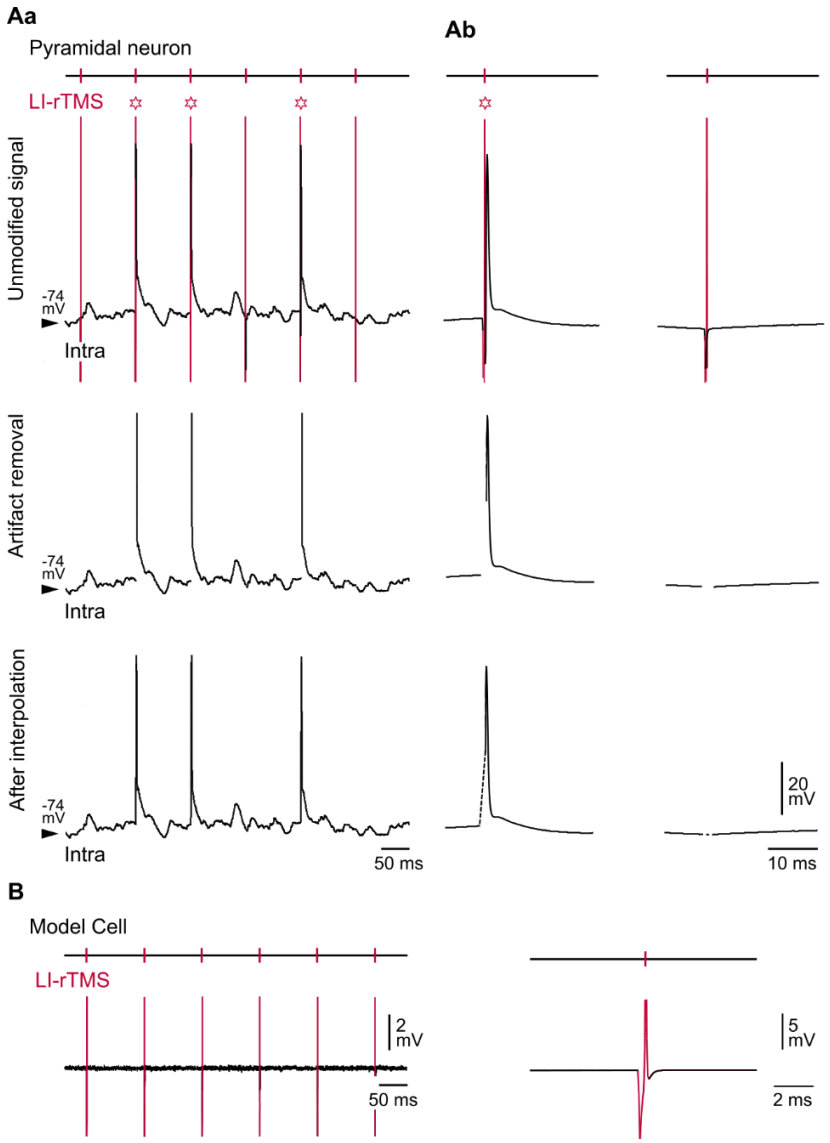


**Fig. S2. Procedure for removing LI-rTMS artifacts.**

**(A)** Off-line cutting and interpolation of electrical artifacts. **(Aa)** Short periods of intracellular activity recorded from a layer 2/3 pyramidal neuron during LI-rTMS, before removal of stimulation artifacts (vertical red lines, Unmodified signal), after their removal (Artifact removal), and after their replacement by linear interpolation (After interpolation). Red stars mark the onset of LI-rTMS-induced AP occurrences. Vm values are indicated at the left of the records. **(Ab)** Left, Representative example of an averaged ($n$ = 2800) LI-rTMS-induced AP before and after removal of the LI-rTMS pulse stimulation artifact. Right, average cell responses ($n$ = 3200) to magnetic pulses in absence of evoked APs. **(B)** Current-clamp recording during LI-rTMS illustrating the

absence of evoked electrical responses in the aftermath of stimulation artifacts (in red) when a CLAMP-1U model cell is simulating the recording of a pyramidal neuron. An expanded view of a single stimulation is shown at right.

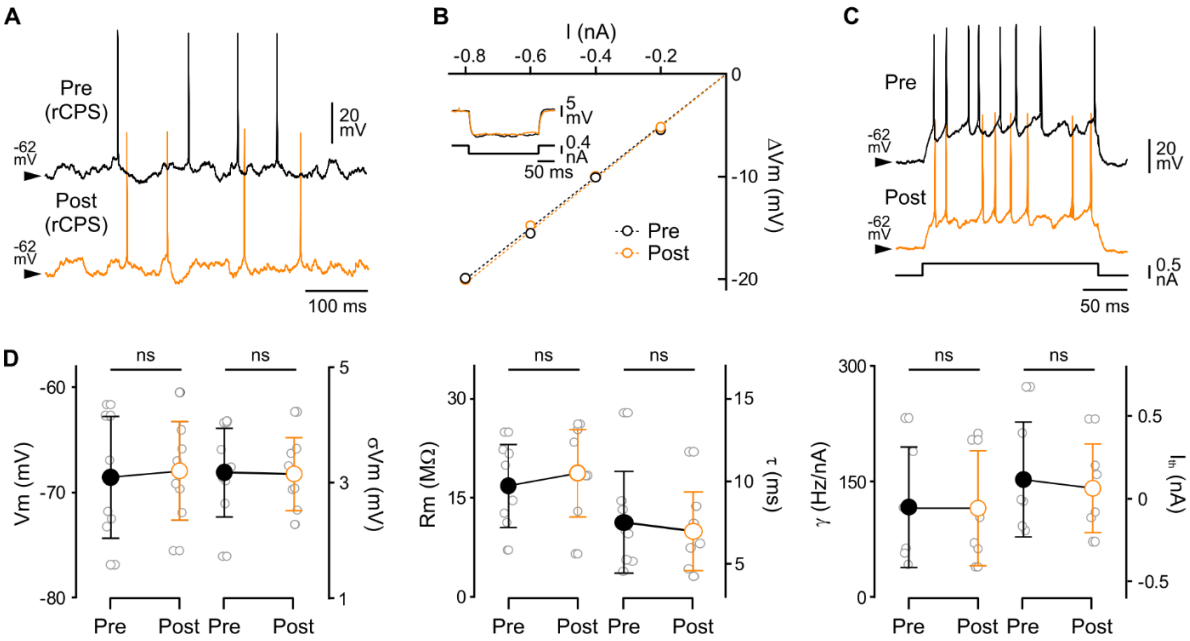


**Fig. S3. Stability of neuronal resting integrative properties and intrinsic excitability after rCPS.**

(**A**) Spontaneous intracellular activity recorded from an S1 neuron before (black trace, Pre) and 15 min after (orange trace, Post) the onset of the rCPS protocol. Vm values are indicated at the left of intracellular records. (**B**) *V–I* relationships computed from the neuron illustrated in (A) before and following the application of the rCPS protocol. The average voltage responses (20–30 trials) to negative current pulses of -0.4 nA (200 ms duration) during pre- and post-stimulation periods are superimposed in the inset. *V–I* relationships were best fitted by linear regressions (dashed colored lines, $r^2 > 0.99$). (**C**) Examples of current-evoked firing responses in baseline (Pre) and following rCPS (Post). (**D**) Population data comparing Vm, σVm, Rm, τm, γ and $I_{th}$ values during the pre- and post-rCPS periods. Gray circles correspond to values of individual neurons and black and orange symbols show the mean ± SD. [Vm: $n = 7$; σVm: $n = 7$; Rm: $n = 6$; τm: $n = 6$; γ: $n = 6$; Ith: $n = 6$; paired Student t-test, ns: non-significant].

| | **Threshold (mV)** | **Amplitude (mV)** | **Duration at mi-amplitude (ms)** | **Peak amplitude (mV)** |
|---|---|---|---|---|
| **Pre (-10 – 0 min.)** | -52.2 ± 1.1 | 59.7 ± 4.6 | 0.66 ± 0.2 | 7.5 ± 4.9 |
| **P1 (+10 – +20 min.)** | -52.5 ± 2.2 | 59.2 ± 5.0 | 0.67 ± 0.2 | 6.4 ± 4.9 |

**Table S1: Properties of spontaneous APs are similar before and after LI-rTMS.**

Values are mean ± SD. No significant difference was found between the pre- and post-stimulation (P1) period ($n$ = 8 neurons; paired Student t-test; $P > 0.16$ for each parameter).